Phosphorylation of Syntaxin 17 by TBK1 controls autophagy initiation

Suresh Kumar[1,2], Yuexi Gu[1,2], Yakubu Princely Abudu[3], Jack-Ansgar Bruun[3], Ashish Jain[4], Farzin Farzam[5], Michal Mudd[1,2], Jan Haug Anonsen[6], Tor Erik Rusten[4], Gary Kasof[7], Nicholas Ktistakis[8], Keith A. Lidke[5], Terje Johansen[3], and Vojo Deretic[1,2 *,**]

[1]Autophagy Inflammation and Metabolism Center of Biomedical Research Excellence,University of New Mexico Health Sciences Center, Albuquerque, NM 87131, USA
[2] Department of Molecular Genetics and Microbiology, University of New Mexico Health Sciences Center, Albuquerque, NM 87131 USA
[3] Molecular Cancer Research Group, Institute of Medical Biology, University of Tromsø - The Arctic University of Norway, 9037 Tromsø, Norway
[4] Department of Molecular Cell Biology, Centre for Cancer Biomedicine, University of Oslo and Institute for Cancer Research, The Norwegian Radium Hospital, N-0379 Oslo, Norway
[5] Departments of Physics and Astronomy, University of New Mexico, Albuquerque, NM 87131, USA
[6] Department of Biosciences IBV Mass Spectrometry and Proteomics Unit, University of Oslo, 0371 Oslo, Norway
[7] Cell Signaling Technology, Danvers, Massachusetts 01923, USA
[8] Signalling Programme, The Babraham Institute, Cambridge CB22 3AT, UK

*Correspondence:
Vojo Deretic, Ph.D.
Professor and Chair
Department of Molecular Genetics and Microbiology
University of New Mexico Health Sciences Center
915 Camino de Salud, NE
Albuquerque, NM 87131
U.S.A.
(505) 272-0291
FAX (505) 272-5309
vderetic@salud.unm.edu

** Lead contact

Summary

The SNARE Syntaxin 17 (Stx17) has been implicated in autophagosome-lysosome fusion. Here we report that Stx17 functions during assembly of protein complexes associated with autophagy initiation. Stx17 is phosphorylated by TBK1 whereby phospho-Stx17 in turn controls formation of the ATG13/FIP200 mammalian pre-autophagosomal structure (mPAS) in response to starvation, a classical inducer of autophagy. TBK1 phosphorylates Stx17 at S202. During autophagy induction, the phosphorylated $Stx17^{pS202}$ transfers from the Golgi, where the steady state pools of phosphorylated Stx17 are localized, to the $ATG13^{+}FIP200^{+}$ mPAS. $Stx17^{pS202}$ was found in complexes with ATG13 and FIP200, whereas its nonphosphorylatable mutant $Stx17^{S202A}$ was not. Stx17 or TBK1 knockouts blocked ATG13 and FIP200 puncta formation. Stx17 knockout reduced formation of ATG13 complexes with FIP200 and ULK1. Endogenous $Stx17^{pS202}$ colocalized with LC3B following induction of autophagy. Stx17 knockout diminished LC3 response and reduced sequestration of the prototypical bulk autophagy cargo lactate dehydrogenase. We conclude that Stx17 is a TBK1 substrate and that phosphorylated Stx17 orchestrates assembly of pre-autophagosomal complexes.

INTRODUCTION

The autophagy pathway controlled by the ATG factors is a cytoplasmic homeostatic process that plays both metabolic and quality control roles, and affects a wide range of physiological and pathological conditions. The known components of the autophagy machinery in mammalian cells include several protein complexes. One such complex contains the first autophagy pathway-dedicated protein kinase ULK1, corresponding to Atg1 in yeast (Chan et al., 2007; Mizushima et al., 2011). The ULK1 complex contains additional components, including FIP200 (Hara et al., 2008) and ATG13 (Alers et al., 2014). These and additional proteins are substrates for upstream kinases, mTOR and AMPK, which regulate the activity of the ULK1 complex in response to the classical inducer of autophagy, starvation (Inoki et al., 2012). In yeast, autophagosomes emanate from the well-defined pre-autophagosomal structure (PAS), whereas the definition of its counterpart in mammalian cells has been elusive.

The ULK1 complex is often considered to be the putative mammalian equivalent of PAS (Mizushima et al., 2011), referred herein as mPAS. The definition of the earliest components that define mPAS has been a topic of much interest, with the FIP200 and ATG13 puncta believed to represent the early precursors of autophagosomes in mammalian cells (Alers et al., 2014; Karanasios et al., 2013; Karanasios et al., 2016; Mizushima et al., 2011; Nishimura et al., 2017). Eventually, these components interact physically or functionally (Dooley et al., 2014; Fujita et al., 2013; Gammoh et al., 2013; Hara et al., 2008) with additional protein systems, including the conjugation machinery that lipidates mammalian Atg8 proteins (mAtg8s), encompassing the well-known member LC3B (Kabeya et al., 2000) that serves as a marker of the early autophagic organelles such as phagophores/isolation membranes as they progress into closed autophagosomes. At several points along this pathway, the class III PI3K VPS34 contributes to the formation and progression of autophagic membrane intermediates, including the initiation events that transit through a structure known as omegasome, marked by the protein DFCP1 (Axe et al., 2008) that binds PI3P, the product of VPS34 (Baskaran et al., 2014; Petiot et al., 2000). Despite this progress, a number of details and the order of events remain to be defined for early stages in autophagy initiation in mammalian cells.

The degradative autophagy pathway culminates in a fusion of closed autophagosomes, after they complete cargo sequestration, with lysosomal organelles where the cargo is eventually degraded (Mizushima et al., 2011). This process is driven by several SNARE complexes including those containing Ykt6 (Bas et al., 2018; Gao et al., 2018; Matsui et al., 2018; Takats et al., 2018) and Stx17 (Diao et al., 2015; Guo et al., 2014; Itakura et al., 2012; Takats et al., 2013; Wang et al., 2016). Initially, it was thought that Stx17 was the main driver of autophagosome-lysosome fusion, but the latest studies indicate that while it contributes to these events, additional SNARE complexes are required (Bas et al., 2018; Gao et al., 2018; Matsui et al., 2018; Takats et al., 2018). The very early studies with Stx17 have also suggested that it functions in a number of ways, including potentially affecting autophagic initiation at the mitochondria-ER contact sites

(Hamasaki et al., 2013) (Arasaki et al., 2018; Arasaki et al., 2015). However, this concept has not received general support.

Another protein kinase, TBK1 (Ahmad et al., 2016), has been implicated in autophagy (Pilli et al., 2012; Thurston et al., 2009; Wild et al., 2011). Some of these studies have focused on interactions between TBK1 and selective autophagy receptors (Thurston et al., 2009; Wild et al., 2011), whereas other studies have suggested a more generalized role in autophagosomal maturation (Pilli et al., 2012) or in trafficking events associated with ATG9 (Saitoh et al., 2009). TBK1 in principle works with a number of adaptors in innate immunity responses such as type I interferon activation (Liu et al., 2015), whereas its interactions with autophagy receptors and regulators expands its repertoire beyond the interferon stimulation.

In this work, we show that TBK1 interacts with and modulates another autophagy factor, Stx17, beside the known selective autophagy receptors. The interaction of Stx17 and TBK1 is further reflected in phosphorylation of Stx17 by TBK1 and modulation of its function. Surprisingly, these interactions and phosphorylation of Stx17 by TBK1 occur at the earliest stages of autophagy, i.e. at its initiation. We demonstrate that phosphorylation of Stx17 is important for assembly of the ULK1 complex and that it is critical for autophagy initiation. We show that phosphorylated Stx17 and components of the ULK1 complex, localized to the Golgi in the resting state, respond to induction of autophagy by translocating from the Golgi to participate in the formation of mPAS during autophagy initiation.

RESULTS

Stx17 and TBK1 interact and TBK1 phosphorylates Stx17 at Ser-202

A set of proteomic analyses (Figure 1A; Table S1) indicated that TBK1 was found in complexes with Stx17. Pull-down experiments comparing GFP vs GFP-Stx17 (Table S1, Tabs 1 and 2) showed 6 or 7 exclusive unique TBK1 peptides (Figure S1A) present only with GFP-Stx17 in 2 out of 3 biological repeats (Figure 1A). This was confirmed by co-immunoprecipitation (co-IP) of endogenous proteins (Figure 1A, bottom panel) and FLAG-Stx17 co-IP with Myc-TBK1 (Fig. 1B). A band with lower electrophoretic mobility (a band shift) recognized by FLAG antibody appeared in FLAG-Stx17 co-IPs with enzymatically active Myc-TBK1 but not in co-IPs with enzymatically dead mutant Myc-TBK1^{K38D} (Figure 1B). Co-expression of FLAG-Stx17 with Myc-tagged proteins (Myc-TBK1 and Myc-TBK1^{K38D}) in TBK1^{KO} HEK293 cells resulted in a similar FLAG-Stx17 mobility shift in cells expressing enzymatically active TBK1 but not in cells expressing TBK1^{K38D} (Figure S1B). A mass spectrometric (MS) analysis of FLAG-Stx17 immunoprecipitates from TBK1^{KO} HEK293 cells identified a precursor ion at m/z 717.3318 corresponding to a triply charged trypsin generated Stx17 peptide IDSIADHVNSAAVNVEEGTK with a phospho-Ser-202 (Stx17^{pS202}) modification (theoretical average at m/z 717.4096). Phosphorylation sites were verified using the PTMrs module in Proteome Discoverer. The MS/MS spectra from Proteome Discoverer indicated that it was Ser-202 that was phosphorylated and not the other potential sites (Table S1, Tab3). The phospho-IDSIADHVNSAAVNVEEGTK (Stx17^{pS202}) peptide was 97-153 and 148-205 times (range from two experiments) more abundant in TBK1 samples relative to samples with Myc or Myc-TBK1^{K38D} (Figure S1C), indicating that TBK1 is a kinase acting on Ser-202 of Stx17. There were additional phosphorylated residues, but they either did not depend on TBK1 or had low post-translational modification probability or low peptide identification confidence.

The Ser-202 residue is within an evolutionarily highly conserved sequence in Stx17 from fish to humans (Figure S1D), located between the SNARE layers +1 and +2 (“1.5”) and predicted to face outwards of the 4-helix bundle (Figure S1E). We raised an antibody against a pSer-202 phosphopeptide spanning this region of Stx17 and obtained antibodies recognizing a band on Western blots that was absent in Stx17 CRISPR knockout HeLa cells (Figures 1D and S1F), and in TBK1 KO HeLa cells (Figure 1D; S1G). The Stx17^{pS202} band was responsive to agonists of TBK1 (muramyl-dipeptide/MDP and LPS), albeit it was also readily detectable in resting cells (Figure S1H). A TBK1 inhibitor BX795 inhibited Stx17 phosphorylation (Stx17^{pS202}) in response to LPS (Figure S1I). Thus, TBK1 phosphorylates Stx17 at Ser202 (Figure 1E).

Phosphorylated Stx17 localizes to the Golgi

Using the antibody against Stx17^{pS202} we found that it labeled specifically Stx17 at the Golgi apparatus. Figure 2A shows that Stx17^{pS202} colocalizes in resting cells with the Golgi marker GM130. The Stx17^{pS202} was not detectable in Stx17 KO cells (Figure 2A) and the

signal was absent in cells pretreated with λ phosphatase (Figure S2A). In TBK1 KO cells, there was still some labeling but the signal was dramatically reduced (Figure S2A). We could not compare Stx17^{pS202} with the distribution of total endogenous Stx17 by immunofluorescence since there are at present no commercial antibodies that can reveal authentic endogenous Stx17, but it is in general known to be in various membranes including ER (Steegmaier et al., 2000; Steegmaier et al., 1998), mitochondria (Arasaki et al., 2015; Hamasaki et al., 2013; Itakura et al., 2012) ER-mitochondria contact sites (Hamasaki et al., 2013), and, when Stx17's putative C-terminal ER retrieval signal sequence (Popoff et al., 2011), KKCS, is deleted, in the Golgi (Itakura et al., 2012). Further confirmation that Stx17^{pS202} localized to the Golgi was established by subcellular membrane fractionation (Figure 2B). Thus, the data shown here indicate that Stx17^{pS202} specifically localizes to the Golgi apparatus.

Upon starvation, which is a classical inducer of autophagy, Stx17^{pS202} translocated from the Golgi to peripheral puncta that were not GM130 positive (Figure 2C). When this was quantified by high content microscopy (HC), a significant reduction in colocalization between Stx17^{pS202} and GM130 was observed (Figure 2D,E), whereas the total number of peripheral Stx17^{pS202} increased (Figure 2F,G). The total level of Stx17^{pS202} did not change with starvation (Figure S2B). Thus, starvation-induced autophagy (Figure S2C,D) is not associated with changes in Stx17^{pS202} levels but is associated with redistribution of Stx17^{pS202} from the Golgi apparatus to peripheral punctate sites (Figure 2H).

Stx17 and TBK1 affect mammalian PAS formation

The intriguing phenotype of Stx17^{pS202} translocation to peripheral puncta during induction of autophagy prompted us to test whether the mPAS formation was affected in Stx17 and TBK1 knockouts. Using ATG13, a component of the mammalian ULK1-ATG13-FIP200 complex often used as an early surrogate marker for mPAS (Ganley et al., 2009; Jung et al., 2009; Karanasios et al., 2013; Karanasios et al., 2016; Koyama-Honda et al., 2013; Lamb et al., 2013), we observed that endogenous ATG13 puncta formation in response to starvation is severely reduced in Stx17^{KO} and TBK1^{KO} cells (Figures 3A-C and S3A). Along with ATG13, another component of the ULK1 autophagosomal initiation complex is FIP200/RB1CC1 (Ganley et al., 2009; Jung et al., 2009). Endogenous FIP200 puncta were also severely reduced in Stx17^{KO} and TBK1^{KO} cells (Figures 3D-F and S3B). The ULK1 puncta (ULK1-GFP) were correspondingly reduced in Stx17^{KO} cells (Figure S3C-E). DFCP1 (Axe et al., 2008) profiles were reduced in Stx17^{KO} and TBK1^{KO} cells (Figures S3F-H). Another well-known marker of early stages of autophagy, WIPI2, displayed reduced number of puncta in Stx17 knockout cells (Figure S3 I-K). Thus, Stx17 and TBK1 are required for formation of mPAS and early autophagosomal intermediate structures.

Only phosphorylatable or phosphomimetic Stx17 can complement ATG13 and FIP200 phenotypes in Stx17 KO cells

We next asked the question of whether Stx17^{KO} can be complemented to restore ATG13 and FIP200 responses to autophagy induction by starvation. We generated phosphomimetic and unphosphorylatable mutants of Stx17, Stx17^{S202D} and Stx17^{S202A}

and used FLAG-Stx17 WT, S202A, and S202D variants in subsequent experiments. Only $Stx17^{WT}$ and $Stx17^{S202D}$ complemented Stx17 KO in HeLa cells, as quantified by HC analysis of cells gated for transfected cells and judged by both markers, ATG13 and FIP200 puncta, in starved cells (Figure 4A-D). Thus, preventing Stx17 from being phosphorylated at the S202 site precludes its functionality in autophagy initiation. Stx17 and its phosphorylation by TBK1 affect autophagy initiation as summarized in Figure 4E.

Phosphorylated Stx17 interacts with ATG13 and FIP200

We next tested whether $Stx17^{pS202}$ associated with members of the mPAS complex. $Stx17^{pS202}$ co-IP'ed with endogenous ATG13 (Figure 5A). It also interacted with FIP200 (Figure 5B). We therefore generated phosphomimetic and unphosphorylatable mutants of Stx17, $Stx17^{S202D}$ and $Stx17^{S202A}$ to test their capacity in these interactions. Only $Stx17^{S202D}$ and wild type Stx17 were found in co-IPs with ATG13 (Figures 5C,D) and FIP200 (Figures 5E,F). We tested whether $Stx17^{pS202}$, which translocates from the Golgi to peripheral sites/puncta (Figure 2B), colocalized with ATG13 upon induction of autophagy. For this, antibodies were not compatible for testing in HeLa cells and thus we resorted to mouse cells, using primary macrophages (bone marrow-derived macrophages; BMMs). In BMMs, $Stx17^{pS202}$ colocalized with ATG13 puncta and this colocalization increased upon induction of autophagy (Figure 5G-I, Figure S4A). $Stx17^{pS202}$ also colocalized with GFP-FIP200 and ULK1-GFP (Figures 5J-O and S4B,D). GFP-FIP200 and $Stx17^{pS202}$ colocalized in resting cells and the colocalization appeared to be in Golgi, where pools of $Stx17^{pS202}$ reside. Subcellular membrane separation showed co-fractionation of FIP200 and $Stx17^{pS202}$ with the Golgi marker GM130 (Fig S4C). Thus, not only does Stx17 affect mPAS components but it also interacts and colocalizes with them (Figure 5P).

Translocation of Stx17 to DFCP1 and LC3 profiles in cells induced for autophagy

We next asked the question whether in cells induced for autophagy, $Stx17^{p202}$ eventually transfers to nascent autophagosomes. Formation of $DFCP1^{+}$ omegasome heralds formation of autophagosomes (Axe et al., 2008). We found that $Stx17^{p202}$ colocalized with DFCP1 (Figure S4E,F), which was tested at a time point later than ATG13 colocalization, compatible with the expectation that ATG13-FIP200 mPAS precedes autophagosome formation. Similarly, $Stx17^{p202}$ colocalized with LC3 (using GFP-LCB; Figure 6A,B). Super-resolution microscopy showed that $Stx17^{p202}$ colocalizes with LC3 at a distance of 40 nm (Figure 6C,D and S5A), which places them very near each other on the autophagosomes, compatible with our prior report of direct binding between Stx17 and mAtg8s (Kumar et al., 2018). HC analyses further confirmed increased colocalization between $Stx17^{p202}$ and LC3B (Figure 6E,F). Mutant forms of Stx17 showed differences in colocalization with LC3B, as quantified by HC: WT and the phosphomimetic $Stx17^{S202D}$ mutant colocalized with LC3B more so than the non-phosphorylatable $Stx17^{S202A}$ mutant (Figures 6G, S5B), reflected also in confocal analyses and Pearson's colocalization coefficients (Figure S5C,D). Furthermore, in cells knocked out for TBK1, there was

reduced association of Stx17 and GFP-LC3B in co-IP experiments (Figure S5E,F). Thus, phosphorylation of Stx17 is important for its colocalization and association with LC3.

Finally, we tested by subcellular fractionation and density separation on OptiPrep gradients where Stx17^{p202} co-fractionates before and after induction of autophagy. We found that most of Stx17^{p202} in resting (full medium) cells co-fractionates with the Golgi marker GM130 (Figure 6H), compatible with our immunofluorescence findings. In contrast, the spread of total Stx17 in gradients was much wider and it was dis-enriched in the Golgi fractions (Figure 6H). Following induction of autophagy by starvation in EBSS, some of Stx17^{p202} translocated to LC3-II (autophagosomal) fractions (Figure 6I). Thus, as determined by various methods, Stx17^{p202} eventually ends in autophagosomal compartments (Figure 6J).

Stx17 is required for efficient assembly of ULK1-ATG13-FIP200 complexes and LC3 puncta formation

We next wondered whether Stx17 affected the formation of ULK1 complexes. HeLa cells knocked out for Stx17 showed less ULK1 in protein complexes with ATG13 when compared to wild type cells (Figure 7A,B). Likewise, HeLa Stx17^{KO} cells showed less FIP200 in complexes with ATG13 (Figure 7C,D). Thus, Stx17 is necessary for efficient formation of components of the mPAS. Further, knockouts of Stx17 and TBK1 reduced LC3 puncta formation at 30 min and 1 h post-induction by starvation. This was tested by monitoring endogenous LC3 response (Figure 7E and S6A). We also used fusion of LC3 with fluorescent proteins to monitor autophagy induction. The GFP-LC3 reporter showed no response in Stx17^{KO} cells, and yet parental wild type cells showed a time response (Figure 7F,G and Figure S6B-D). Using Keima-LC3 (An and Harper, 2018; Katayama et al., 2011), we also observed fewer fluorescent puncta detected by excitation at 440 nm in Stx17^{KO} cells relative to wild type cells (Figure 7H,I). Thus, Stx17 matters for autophagy initiation.

Stx17 is required for efficient bulk autophagy cargo sequestration

If Stx17 is important for autophagosomal initiation, and not only for autophagosome-lysosome fusion as previously reported (Itakura et al., 2012), one prediction is that Stx17^{KO} cells would display less bulk autophagy cargo sequestration. A classical cargo for this is uptake of cytosolic lactate dehydrogenase (LDH) into autophagosomes, that can be tested in a well-established cargo sequestration assay (Kopitz et al., 1990; Pattingre et al., 2003; Seglen and Gordon, 1984; Seglen et al., 2015) Employing this assay, we found that Stx17^{KO} reduced LDH sequestration in autophagosomes comparably to the reduction in cargo sequestration caused by a knockout in ATG13 (Figure S6E), or upon treatment of WT cells with classical inhibitor of autophagy 3MA (Figure 7J,K). Published knockouts (Nguyen et al., 2016) of mAtg8s in combinations as triple LC3A-C combination, or triple GABARAPs (GABARAP, L1 and L2), or all six mAtg8s (Hexa) also reduced LDH sequestration (Figure 7L and S6F), albeit the effect of LC3 triple knockouts was milder than effects of GABARAP triple knockouts and Hexa knockout cells, in keeping with a prior report (Engedal and Seglen, 2016; Szalai et al., 2015). In all

the above experiments the cells were inhibited for autophagosomal maturation using Bafilomycin A1. We also employed LDH-mKeima construct (An and Harper, 2018) and observed reduced Keima fluorescence at 440 nm (excitation) in Stx17^{KO} cells (Figure 7M,N). Thus, Stx17 is necessary for autophagy initiation and for the sequestration of nonselective, bulk autophagy cargo into non-degradative early autophagosomal organelles.

DISCUSSION

Here, we found that Stx17 is a substrate for TBK1 phosphorylation and that both TBK1 and Stx17 play a role in autophagy initiation. The phosphorylated form of Stx17 is localized to the Golgi in resting cells. During induction of autophagy, these pools of Stx17 redistribute from the Golgi to peripheral vesicles, which are the likely sites contributing to pre-autophagosomal structures, i.e. the FIP200 and ATG13 puncta, the early precursors of autophagosomes in mammalian cells (Alers et al., 2014; Karanasios et al., 2013; Karanasios et al., 2016; Mizushima et al., 2011; Nishimura et al., 2017). Phosphorylation of Stx17 is necessary for efficient formation of the ATG13 and FIP200 puncta in response to starvation, and Stx17 is required for robust interactions between components of the FIP200-ATG13-ULK1 complex. Stx17 knockout cells do not respond to autophagy induction, reflected in diminished LC3 puncta formation and reduced sequestration of LDH, a classical substrate for starvation-induced bulk autophagy (Kopitz et al., 1990; Pattingre et al., 2003; Seglen and Gordon, 1984; Seglen et al., 2015). Thus, TBK1 and Stx17 cooperate in autophagy initiation during starvation responses.

TBK1, a kinase often associated with immune responses such as type I interferon induction and with roles in cancer and neurodegeneration (Ahmad et al., 2016), has been implicated in autophagy in several ways including interactions with or phosphorylation of autophagy receptors such as NDP52 (Thurston et al., 2009), Optineurin (Wild et al., 2011) and p62 (Pilli et al., 2012). Our present study shows that TBK1 has additional substrates implicated in autophagy, such as Stx17. Previously, both TBK1 (Pilli et al., 2012) and Stx17 (Itakura et al., 2012) have been shown to play a role in autophagy maturation. Our new findings do not contradict this role, but indicate that TBK1 plays a role at multiple stages of autophagy, as already evident from modifications of selective autophagy receptors by TBK1 (Wild et al., 2011).

Stx17 has been well studied in the context of autophagy maturation (Diao et al., 2015; Guo et al., 2014; Itakura et al., 2012; Takats et al., 2013; Wang et al., 2016), although more recent studies have implicated additional SNAREs, such as Ykt6, in autophagosome-lysosome fusion (Bas et al., 2018; Gao et al., 2018; Matsui et al., 2018; Takats et al., 2018). Furthermore, Stx17 has diverse functions, some of which are compatible with autophagy initiation (Arasaki et al., 2018; Hamasaki et al., 2013). These additional roles include various processes such as mitochondrial fission (Arasaki et al., 2015), fusion with lysosomes of specialized mitochondria-derived vesicles (McLelland et al., 2016), and fusion of ER-derived vesicles with lysosomes (Fregno et al., 2018), the

latter being compatible with the early description of Stx17 localization to the ER (Steegmaier et al., 2000).

Our findings place Stx17^{pS202} at the Golgi. It has previously been shown that mutation of the putative ER-retrieval signal at the C-terminus of Stx17 leads to re-localization of the bulk Stx17 to the Golgi (Itakura et al., 2012). It is possible that the phosphorylated form of Stx17 conformationally escapes recognition by COPI-dependent ER-retrieval machinery (Popoff et al., 2011). Our MS analyses (Table S1), indicate extensive interactions of Stx17 with the components of the COPI complex (COPA, COPB2, COPG2 and COPG1), in keeping with the above trafficking routes of Stx17.

Upon autophagy induction, Stx17^{pS202} translocates from the Golgi to the peripheral pools where it colocalizes with FIP200, ATG13, and ULK1. Of interest is that FIP200, like Stx17^{pS202}, co-fractionates with the Golgi membranes. It is possible that a fraction of FIP200 destined for mPAS translocates via a route related to that of Stx17^{pS202}. The Golgi apparatus appears to serve as a depot of Stx17 and possibly of FIP200 until they are needed at the sites of autophagosome formation. This is similar to the presence of ATG9 in the Golgi (Saitoh et al., 2009; Young et al., 2006) until it is mobilized into peripheral Atg9 vesicular pools (Lamb et al., 2016; Soreng et al., 2018). Of note, TBK1 responds to various inputs, in combinations with different receptors/adaptors it interacts with (Liu et al., 2015), and thus Stx17 could play a role of a novel adaptor/effector for TBK1. One of the previously defined pathways with well-studied adaptors (Liu et al., 2015), includes STING, which traffics from the ER to the Golgi and then to post-Golgi compartments (Saitoh et al., 2009). It is likely that Stx17 and TBK1 intersect at some point along such routes. Of note, the response to starvation is not linked to phosphorylation of Stx17 by TBK1, which appears tonic in nature and is prominently present in resting cells. Rather, starvation induces trafficking events relocating phosphorylated Stx17 from the Golgi to mPAS. The mechanism of this is unknown at present, but may share the Atg9 route or depend on another membrane trafficking pathway.

We previously reported that Stx17 interacts with LC3 (Kumar et al., 2018), further extended here to the phosphorylated form of Stx17, Stx17^{pS202}. Since TBK1 knockout reduced this interaction, it is likely that phosphorylation by TBK1 of Stx17, affects the ability of Stx17 to associate with early autophagosomal structures, possibly contributing to transitions between mPAS and LC3-positive autophagosomes. In support of this view is the finding that Stx17^{pS202} also colocalizes with DFCP1, a marker for an intermediate omegasome structure from which nascent autophagosomes emerge (Axe et al., 2008). Thus, Stx17 transits sequential sites along the autophagosomal pathway.

The interconnections between different parts of autophagy initiation machinery have several well-known precedents. For example, FIP200 links the ULK1 complexes (Hara et al., 2008) with ATG16L1 (Fujita et al., 2013; Gammoh et al., 2013), and hence connects the LC3 conjugation machinery with the mPAS. Furthermore, WIPI2, a PI3P-binding factor, directly interacts with ATG16L1 (Dooley et al., 2014). Stx17 may provide further links, as Stx17 is known to bind ATG14L (Arasaki et al., 2018; Diao et al., 2015), a component of the PI3K complex engaged in autophagy initiation. Our findings that Stx17

interacts with FIP200-ATG13-ULK1, and our previous report that it can bind unlipidated LC3/mAtg8s (Kumar et al., 2018), suggest the possibility that Stx17 may present LC3/mAtg8s as substrates to the conjugation/lipidation machinery. However, other roles for LC3 binding to the Stx17 SNARE domain are possible, such as temporarily blocking Stx17's engagement in a premature SNARE bundle assembly until the later stages, i.e. maturation. The incorporation of Stx17 at the outset, within the autophagy complexes governing the earliest stages of autophagosome formation, coordinates initiation with subsequent autophagy stages culminating in fusion with the lysosome. This ensures that once the cargo sequestration process is initiated it can be completed to accomplish its degradative role.

MATERIALS AND METHODS

Antibodies and reagents

The following antibodies and dilutions were used: Stx17 (Sigma, HPA001204; 1:1000 (WB)); Flag (mouse monoclonal Sigma; F1804, used at 0.5 µg/ml and 1:1,000 for (WB); 1:250 (IF)); GFP (rabbit Abcam; ab290; 0.5 µg/ml IP and 1:4,000 (WB)); LC3 (rabbit; MBL International PM036, 1:500 (IF); ATG13 (rabbit; Cell Signaling Technology; 13468, 1:1000 (WB); 1:150 (IF); ATG13 (mouse Millipore; MABC46, 1:200 (IF); FIP200 (rabbit; Proteintech; 17250-1-AP, 1:200 (IF)); TBK1(rabbit Cell Signaling Technology; 3504, 1:1000 (WB); 1:200 (IP)); pTBK1S172 (rabbit Cell Signaling Technology; 5483, 1:1000 (WB)); FIP200 (rabbit Cell Signaling Technology; 12436, 1:1000 (WB)); ULK1 (rabbit Cell Signaling Technology; 6439, 1:750 (WB); Stx17^{pS202} (rabbit Cell Signaling Technology (customized), 1:250 (IF); 1:1000 (WB); Lambda Protein Phosphatase (NEW ENGLAND BioLabs Inc.; P0753S); GM 130 (mouse BD Biosciences, RUO-610822, 1:500 (IF)); Dynabeads Protein G (Thermo Fisher Scientific 10003D 50µl/ IP); Bafilomycin A1 (Baf A1, InvivoGen, 13D02-MM); OptiPrep Density Gradient Medium (Sigma, D1556); Lipofectamin 2000, Thermo Scientific, 11668019; Goat anti mouse IRDye 680 (LI-COR, 925-68020);Goat a Rabbit IRDye 800 (LI-COR, 926-32211); Trueblot anti-mouse DyLight 680, (Rockland, 18-4516-32); Trueblot anti-rabbit DyLight 800 (Rockland, 18-8816-31).

Cell culture

HEK 293T and HeLa cells were obtained directly from ATCC and maintained in ATCC recommended media. Mouse bone marrow macrophages (BMMs) were extracted from mouse bone marrow and cultured in DMEM media supplemented with high glucose, sodium bicarbonate and 20% FBS.

Plasmids transfections

PCR products were amplified from cDNA using Phusion High-Fidelity DNA polymerase with primers containing the Gateway recombination site or restriction enzyme sites for the Gateway entry vector and cloned into pDONR221 using Gateway recombination cloning. Plasmids were generated using conventional restriction enzyme cloning and/or by the Gateway recombination system (Invitrogen). Point-mutants were generated using the QuikChange Site-directed Mutagenesis Kit (Agilent, 200523). Plasmid constructs were verified by conventional restriction enzyme digestion and/or by DNA-sequencing. Plasmids were transfected using ProFection Mammalian Transfection System from Promega or using Lipofectamine 2000 (Thermo Scientific).

Mass spectrometric analysis of Stx17 phosphorylation by TBK1

TBK1 Knockout HEK293 cells were transfected with FLAG-STX17 and cotransfected with either empty Myc-tag vector, wild-type Myc-TBK1 or kinase-dead mutant Myc-TBK1 K38D. Cells were lysed and lysates were incubated with anti-FLAG M2 affinity agarose gel (Sigma-Aldrich, # A2220) for 2 hr and washed three times with Lysis buffer. Bound proteins were eluted by boiling in 2x SDS loading buffer for 10 mins. Eluted proteins were separated on SDS-PAGE. Gel pieces were subjected to in gel reduction with DTT, alkylation with Iodoacetamide, and digestion using 6 ng/µl trypsin (Promega, #V511A) or chymotrypsin (Promega, #V1062) (Shevchenko et al., 1996). Peptide mixtures containing

0.1% formic acid were loaded onto a Thermo Fisher Scientific EASY-nLC1000 system and EASY-Spray column (C18, 2µm, 100 Å, 50µm, 50 cm). Peptides were fractionated using a 2-100% acetonitrile gradient in 0.1 % formic acid over 50 min at a flow rate of 250 nl/min. The separated peptides ware analysed using a Thermo Scientific Q-Exactive™ mass spectrometer. Data were collected in data dependent mode using a Top10 method. Processing of raw data was done using the Thermo Scientific Proteome Discoverer 2.2 software. The fragmentation spectra were searched against the current Uniprot database using an in-house Mascot server (Matrix Sciences, UK). Peptide mass tolerances used in the search were 10 ppm, and fragment mass tolerance was 0.02 Da. Methionine oxidation and carbamidomethylation was set as variable modifications. Phosphorylation sites were verified using the PTMrs module in Proteome Discoverer™. Visualization of mass spectra was done with the Thermo Scientific Xcalibur™ software.

Mass spectrometric analysis of Stx17 interactors

HEK293T cells were transfected with plasmids (pDest-EGFP or pDest-EGFP-Stx17) using Lipofectamine 2000 and Immunoprecipitation was performed 48 h after transfection using ChromoTek GFP-Trap following the supplier's instructions. Immuno-precipitated (IPed) samples were loaded on a 12% polyacrylamide- gel and Coomassie stained. Subsequently each lane was cut into 5 slices and destained. Reduction, alkylation and proteinase digestion was carried out with trypsin overnight at 37ºC as previously described (Faeste et al., 2014; Faeste et al., 2016). Subsequent extraction of protease-generated peptides was performed as previously described (Anonsen et al., 2012). Analyses of in-gel digested peptides were done by reverse phase nanoflow liquid chromatography coupled to a nanoelectrospray QExactive mass spectrometer utilizing a Higher energy induced dissociation (HCD) fragmentation (RP nLC-ESI MS2). The RP nLC was performed as previously described (Faeste et al., 2016). Raw files data were analyzed with Proteome Discoverer (v.1.4.7) utilizing the SEQUEST search engine and with MASCOT (version 2.4.0, Matrix Science, London, UK). Trypsin was selected as enzyme for samples treated with the respective enzymes allowing one missed cleavage site. Tolerance of 10 ppm for the precursor ion in the first search and 0.05 Da for the MS/MS fragments was applied. In addition to methionine oxidation, acetylation at protein N-terminus was allowed as variable modifications. Cysteine carbamidomethylation was set as fixed modification. High confidence peptides set at FDR <0.01 and medium confidence peptide set at FDR <0.05. Quantitative analyses using spectral counting were performed with Scaffold (version, 4.4.0, Proteome Software Inc., Portland, OR, USA).
Peptide identifications were accepted at greater than 95.0% probability and Protein identifications were accepted at greater than 99.0% probability. Only proteins with >1 peptide identification were considered for quantitation.

Generation of CRISPR mutant cells

Stx17 and ATG13 CRISPR in HeLa cells were generated as described earlier (Kumar et al., 2018). Briefly, the lentiviral vector carrying both Cas9 enzyme and a gRNA targeting Stx17 (GATAGTAATCCCAACAGACC), and ATG13 (TCACCCTAGTTATAGCAAGA) were transfected into HEK293T cells together with the packaging plasmids psPAX2 and pCMV-VSV-G at the ratio of 5: 3: 2. Two days after transfection, the supernatant containing lentiviruses was collected and used to infect the cells. 36 hours after infection,

the cells were treated with puromycin (1 mg/ml) for one week to select Stx17-knockout cells. The knockouts were confirmed by western blotting. To generate TBK1 KO cells in HeLa and HEK293 cells, TBK1 gRNA (GATGAAGATCAACCTGGAAG) was annealed and ligated into a Bbs1 linearized PX459 vector (Addgene #62988) carrying both a wild-type Cas9 and puromycin resistance genes. The gRNA containing vector was transfected into both cells using Mectafectene Pro (Biontex #T020). 24 hours after transfection, cells were treated with 1µg/ml of puromycin for 36hrs to select transfected cells. Following selection, single cells were sorted into 96-well plates and expanded. The KO cells were confirmed by immunoblotting.

High content microscopy

Cells were plated in 96 well plates and were transfected with plasmids whenever required. Cells were stimulated for autophagy by incubating in EBSS for 1h or 2h followed by fixation with 4% paraformaldehyde for 10 mins. Cells were permeabilized with 0.1% saponin and blocked in 3% BSA for 20 mins followed by incubation with primary antibody for 4 h and secondary antibody for 1 h. High content microscopy with automated image acquisition and quantification was carried out using a Cellomics HCS scanner and iDEV software (Thermo) in 96-well plates (Mandell et al., 2014).

High content microscopy for Keima probes

WT HeLa, Stx17^{KO} or TBK1^{KO} cells were plated in 96 well plates and transfected with indicated Keima plasmids. Cells were incubated in full media or induced for autophagy by incubating with EBSS for 2h. After 2h cells were incubated in full media and incubated with Hoechst 33342 for ten minutes in full media and then acquired for Keima fluorescence at 440nm and 560 nm using the Cell Insight CX7 High-Content Screening (HCS) Platform (Thermo).

Super-resolution microscopy

Super-resolution imaging, and analysis were done as described previously (Kumar et al., 2018). HeLa cells were plated on 25 mm round coverslips (Warner instruments) and allowed to adhere overnight, followed by transfection with GFP-LC3B plasmid. Cells were induced for autophagy by incubating with EBSS for 2h. After fixation, cells were incubated with anti-rabbit-Stx17^{pS202} antibody for 4h and washed with PBS, followed by labeling with Alexa Fluor 647 (Invitrogen, A21245). The coverslip was mounted on an Attofluor cell chamber (A-7816, life technologies) with 1.1 ml of the imaging buffer. The imaging and center-to-center distances between GFP-LC3B and Stx17^{pS202} cluster centroids per ROI (region of interest) were calculated as described earlier (Kumar et al., 2018).

Immunofluorescence confocal microscopy

For immunofluorescence confocal microscopy, cells were plated onto coverslips in 12-well plates. Cells were transfected with plasmids indicated in figures. Transfected cells were incubated in full media or EBSS (Earle's Balanced Salt Solution) for times indicated in figures and fixed in 4% paraformaldehyde for 10 min followed by permeabilization with 0.1% saponin in 3% BSA. Cells were then blocked in PBS containing 3% BSA and then incubated with primary antibodies for 4h. Cells were washed three times with PBS and then incubated with appropriate secondary antibodies (Invitrogen) for 1 h at room

temperature. Coverslips were then mounted using ProLong Gold Antifade Mountant (Invitrogen) and analyzed by confocal microscopy using the Zeiss LSM510 Laser Scanning Microscope.

Lactate dehydrogenase (LDH) sequestration assay

LDH sequestration assay was done as described previously (Pattingre et al., 2003); (Seglen et al., 2015). Briefly, 3×10^6 $Hela^{WT}$, $Stx17^{KO}$ or $ATG13^{KO}$ cells were plated in 10 cm dishes, induced for autophagy using EBSS in presence of Bafilomycin A1 for 2 h. Cells were collected and washed twice with phosphate-buffered saline and then once with homogenization buffer (50 mM potassium phosphate, 1 mM EDTA, 1 mM dithiothreitol, 1 mM phenylmethylsulfonyl fluoride (PMSF), 300 mM sucrose, 100 µg/ml bovine serum albumin, and 0.01% Tween 20. Cells were homogenized in 1 ml of cold homogenization buffer by 15 strokes in a glass/Teflon homogenizer on ice, followed by centrifugation at 300 ×*g* for 10 min at 4 °C. Post-nuclear material was layered on 3.5 ml of buffered Nycodenz/ sucrose (10% sucrose, 8% Nycodenz, 1 mM EDTA, 100 µg/ml bovine serum albumin, and 0.01% Tween 20) and centrifuged at 7000× *g* for 1h. The pellet was washed with homogenization buffer and resuspended in buffer containing 2 mM Tris-HCl (pH 7.4), 50 mM mannitol, 1 mM PMSF, 0.5 µg/ml leupeptin, 0.1 µg/ml aprotinin, and 0.7 ug/ml pepstatin. The suspension was sonicated and centrifuged at 15,000 ×*g* for 10 min. The lactate dehydrogenase activity was measured using an LDH assay kit from Promega using manufacture's protocols.

Membrane fractionation

Membrane fractionation was carried out as described previously (Ge et al., 2013; Kumar et al., 2018). Briefly, HEK 293T cells (5 dishes per sample) were plated in 10 cm dishes, harvested, and homogenized by passing through a 22-G needle. Homogenates were subjected to sequential differential centrifugation at 3,000 × g (10 min) and 25,000 × g (20 min) to collect the pelleted membranes (TLA100.3 rotor, Beckman, polypropylene tube; Beckman). 25K membrane pellets were suspended in 1 ml 19% OptiPrep for a step gradient containing 0.5 ml 22.5%, 1 ml 19% (sample), 0.9 ml 16%, 0.9 ml 12%, 1 ml 8%, 0.5 ml 5% and 0.2 ml 0% OptiPrep each. The OptiPrep gradient was centrifuged at 150,000 x g for 3 h and subsequently eight fractions, 0.5 ml each, were collected from the top. Fractions were diluted with B88 buffer (20 mM Hepes, pH 7.2, 150 mM potassium acetate, 5 mM magnesium acetate, 250 mM sorbitol) and membranes were collected by centrifugation at 100,000 x g for 1 h. Sample were subjected to SDS-PAGE and western blot for Stx17, $Stx17^{pS202}$, GM130 and LC3 was done as described under immunoblotting.

Immunobloting and co-immunoprecipitation assays

Immunoblotting and co-immunoprecipitation (co-IP) were performed as described previously (Chauhan et al., 2016). For co-IP, cells were transfected with 10 µg of plasmids, wherever stated, and lysed in NP-40 buffer containing protease inhibitor cocktail (Roche, cat# 11697498001) and PMSF (Sigma, cat# 93482). Lysates were mixed with 2-5 µg antibody and incubated at 4°C for 4 h followed by incubation with Dynabeads protein G (Life Technologies) for 2 h at 4°C. Beads were washed three times with PBS and then boiled with SDS-PAGE buffer for analysis of interacting protein by immunoblotting.

Statistical analyses
Data are expressed as means ± SEM (n ≥ 3). Data were analyzed with a paired two-tailed Student's *t*-test or analysis of variance (ANOVA) was used. Statistical significance was defined as *$P < 0.05$, **$p<0.01$.

Acknowledgments
This work was supported by NIH grants 2R37AI042999-21 and R01AI042999-5 and center grant P20GM121176-01 to V.D., and by grant 249884 from the Research Council of Norway to T.J.

REFERENCES

Ahmad, L., Zhang, S.Y., Casanova, J.L., and Sancho-Shimizu, V. (2016). Human TBK1: A Gatekeeper of Neuroinflammation. Trends Mol Med *22*, 511-527.

Alers, S., Wesselborg, S., and Stork, B. (2014). ATG13: just a companion, or an executor of the autophagic program? Autophagy *10*, 944-956.

An, H., and Harper, J.W. (2018). Systematic analysis of ribophagy in human cells reveals bystander flux during selective autophagy. Nat Cell Biol *20*, 135-143.

Anonsen, J.H., Egge-Jacobsen, W., Aas, F.E., Borud, B., Koomey, M., and Vik, A. (2012). Novel protein substrates of the phospho-form modification system in Neisseria gonorrhoeae and their connection to O-linked protein glycosylation. Infect Immun *80*, 22-30.

Arasaki, K., Nagashima, H., Kurosawa, Y., Kimura, H., Nishida, N., Dohmae, N., Yamamoto, A., Yanagi, S., Wakana, Y., Inoue, H.*, et al.* (2018). MAP1B-LC1 prevents autophagosome formation by linking syntaxin 17 to microtubules. EMBO Rep.

Arasaki, K., Shimizu, H., Mogari, H., Nishida, N., Hirota, N., Furuno, A., Kudo, Y., Baba, M., Baba, N., Cheng, J.*, et al.* (2015). A role for the ancient SNARE syntaxin 17 in regulating mitochondrial division. Dev Cell *32*, 304-317.

Axe, E.L., Walker, S.A., Manifava, M., Chandra, P., Roderick, H.L., Habermann, A., Griffiths, G., and Ktistakis, N.T. (2008). Autophagosome formation from membrane compartments enriched in phosphatidylinositol 3-phosphate and dynamically connected to the endoplasmic reticulum. J Cell Biol *182*, 685-701.

Bas, L., Papinski, D., Licheva, M., Torggler, R., Rohringer, S., Schuschnig, M., and Kraft, C. (2018). Reconstitution reveals Ykt6 as the autophagosomal SNARE in autophagosome-vacuole fusion. J Cell Biol.

Baskaran, S., Carlson, L.A., Stjepanovic, G., Young, L.N., Kim do, J., Grob, P., Stanley, R.E., Nogales, E., and Hurley, J.H. (2014). Architecture and dynamics of the autophagic phosphatidylinositol 3-kinase complex. Elife *3*.

Chan, E.Y., Kir, S., and Tooze, S.A. (2007). siRNA screening of the kinome identifies ULK1 as a multidomain modulator of autophagy. J Biol Chem *282*, 25464-25474.

Chauhan, S., Kumar, S., Jain, A., Ponpuak, M., Mudd, M.H., Kimura, T., Choi, S.W., Peters, R., Mandell, M., Bruun, J.A.*, et al.* (2016). TRIMs and Galectins Globally

Cooperate and TRIM16 and Galectin-3 Co-direct Autophagy in Endomembrane Damage Homeostasis. Dev Cell *39*, 13-27.

Diao, J., Liu, R., Rong, Y., Zhao, M., Zhang, J., Lai, Y., Zhou, Q., Wilz, L.M., Li, J., Vivona, S.*, et al.* (2015). ATG14 promotes membrane tethering and fusion of autophagosomes to endolysosomes. Nature *520*, 563-566.

Dooley, H.C., Razi, M., Polson, H.E., Girardin, S.E., Wilson, M.I., and Tooze, S.A. (2014). WIPI2 Links LC3 Conjugation with PI3P, Autophagosome Formation, and Pathogen Clearance by Recruiting Atg12-5-16L1. Mol Cell *55*, 238-252.

Engedal, N., and Seglen, P.O. (2016). Autophagy of cytoplasmic bulk cargo does not require LC3. Autophagy *12*, 439-441.

Faeste, C.K., Jonscher, K.R., Dooper, M.M., Egge-Jacobsen, W., Moen, A., Daschner, A., Egaas, E., and Christians, U. (2014). Characterisation of potential novel allergens in the fish parasite Anisakis simplex. EuPA Open Proteom *4*, 140-155.

Faeste, C.K., Moen, A., Schniedewind, B., Haug Anonsen, J., Klawitter, J., and Christians, U. (2016). Development of liquid chromatography-tandem mass spectrometry methods for the quantitation of Anisakis simplex proteins in fish. J Chromatogr A *1432*, 58-72.

Fregno, I., Fasana, E., Bergmann, T.J., Raimondi, A., Loi, M., Solda, T., Galli, C., D'Antuono, R., Morone, D., Danieli, A.*, et al.* (2018). ER-to-lysosome-associated degradation of proteasome-resistant ATZ polymers occurs via receptor-mediated vesicular transport. EMBO J *37*.

Fujita, N., Morita, E., Itoh, T., Tanaka, A., Nakaoka, M., Osada, Y., Umemoto, T., Saitoh, T., Nakatogawa, H., Kobayashi, S.*, et al.* (2013). Recruitment of the autophagic machinery to endosomes during infection is mediated by ubiquitin. J Cell Biol *203*, 115-128.

Gammoh, N., Florey, O., Overholtzer, M., and Jiang, X. (2013). Interaction between FIP200 and ATG16L1 distinguishes ULK1 complex-dependent and -independent autophagy. Nat Struct Mol Biol *20*, 144-149.

Ganley, I.G., Lam du, H., Wang, J., Ding, X., Chen, S., and Jiang, X. (2009). ULK1.ATG13.FIP200 complex mediates mTOR signaling and is essential for autophagy. J Biol Chem *284*, 12297-12305.

Gao, J., Reggiori, F., and Ungermann, C. (2018). A novel in vitro assay reveals SNARE topology and the role of Ykt6 in autophagosome fusion with vacuoles. J Cell Biol.

Ge, L., Melville, D., Zhang, M., and Schekman, R. (2013). The ER-Golgi intermediate compartment is a key membrane source for the LC3 lipidation step of autophagosome biogenesis. Elife *2*, e00947.

Guo, B., Liang, Q., Li, L., Hu, Z., Wu, F., Zhang, P., Ma, Y., Zhao, B., Kovacs, A.L., Zhang, Z.*, et al.* (2014). O-GlcNAc-modification of SNAP-29 regulates autophagosome maturation. Nat Cell Biol *16*, 1215-1226.

Hamasaki, M., Furuta, N., Matsuda, A., Nezu, A., Yamamoto, A., Fujita, N., Oomori, H., Noda, T., Haraguchi, T., Hiraoka, Y.*, et al.* (2013). Autophagosomes form at ER-mitochondria contact sites. Nature *495*, 389-393.

Hara, T., Takamura, A., Kishi, C., Iemura, S., Natsume, T., Guan, J.L., and Mizushima, N. (2008). FIP200, a ULK-interacting protein, is required for autophagosome formation in mammalian cells. J Cell Biol *181*, 497-510.

Inoki, K., Kim, J., and Guan, K.L. (2012). AMPK and mTOR in cellular energy homeostasis and drug targets. Annu Rev Pharmacol Toxicol *52*, 381-400.

Itakura, E., Kishi-Itakura, C., and Mizushima, N. (2012). The hairpin-type tail-anchored SNARE syntaxin 17 targets to autophagosomes for fusion with endosomes/lysosomes. Cell *151*, 1256-1269.

Jung, C.H., Jun, C.B., Ro, S.H., Kim, Y.M., Otto, N.M., Cao, J., Kundu, M., and Kim, D.H. (2009). ULK-Atg13-FIP200 complexes mediate mTOR signaling to the autophagy machinery. Mol Biol Cell *20*, 1992-2003.

Kabeya, Y., Mizushima, N., Ueno, T., Yamamoto, A., Kirisako, T., Noda, T., Kominami, E., Ohsumi, Y., and Yoshimori, T. (2000). LC3, a mammalian homologue of yeast Apg8p, is localized in autophagosome membranes after processing. Embo J *19*, 5720-5728.

Karanasios, E., Stapleton, E., Manifava, M., Kaizuka, T., Mizushima, N., Walker, S.A., and Ktistakis, N.T. (2013). Dynamic association of the ULK1 complex with omegasomes during autophagy induction. J Cell Sci *126*, 5224-5238.

Karanasios, E., Walker, S.A., Okkenhaug, H., Manifava, M., Hummel, E., Zimmermann, H., Ahmed, Q., Domart, M.C., Collinson, L., and Ktistakis, N.T. (2016). Autophagy initiation by ULK complex assembly on ER tubulovesicular regions marked by ATG9 vesicles. Nature communications *7*, 12420.

Katayama, H., Kogure, T., Mizushima, N., Yoshimori, T., and Miyawaki, A. (2011). A sensitive and quantitative technique for detecting autophagic events based on lysosomal delivery. Chem Biol *18*, 1042-1052.

Kopitz, J., Kisen, G.O., Gordon, P.B., Bohley, P., and Seglen, P.O. (1990). Nonselective autophagy of cytosolic enzymes by isolated rat hepatocytes. J Cell Biol *111*, 941-953.

Koyama-Honda, I., Itakura, E., Fujiwara, T.K., and Mizushima, N. (2013). Temporal analysis of recruitment of mammalian ATG proteins to the autophagosome formation site. Autophagy *9*, 1491-1499.

Kumar, S., Jain, A., Farzam, F., Jia, J., Gu, Y., Choi, S.W., Mudd, M.H., Claude-Taupin, A., Wester, M.J., Lidke, K.A*., et al.* (2018). Mechanism of Stx17 recruitment to autophagosomes via IRGM and mammalian Atg8 proteins. J Cell Biol *217*, 997-1013.

Lamb, C.A., Nuhlen, S., Judith, D., Frith, D., Snijders, A.P., Behrends, C., and Tooze, S.A. (2016). TBC1D14 regulates autophagy via the TRAPP complex and ATG9 traffic. EMBO J *35*, 281-301.

Lamb, C.A., Yoshimori, T., and Tooze, S.A. (2013). The autophagosome: origins unknown, biogenesis complex. Nat Rev Mol Cell Biol *14*, 759-774.

Liu, S., Cai, X., Wu, J., Cong, Q., Chen, X., Li, T., Du, F., Ren, J., Wu, Y.T., Grishin, N.V*., et al.* (2015). Phosphorylation of innate immune adaptor proteins MAVS, STING, and TRIF induces IRF3 activation. Science *347*, aaa2630.

Mandell, M.A., Jain, A., Arko-Mensah, J., Chauhan, S., Kimura, T., Dinkins, C., Silvestri, G., Munch, J., Kirchhoff, F., Simonsen, A*., et al.* (2014). TRIM proteins regulate autophagy and can target autophagic substrates by direct recognition. Dev Cell *30*, 394-409.

Matsui, T., Jiang, P., Nakano, S., Sakamaki, Y., Yamamoto, H., and Mizushima, N. (2018). Autophagosomal YKT6 is required for fusion with lysosomes independently of syntaxin 17. J Cell Biol *217*, 2633-2645.

McLelland, G.L., Lee, S.A., McBride, H.M., and Fon, E.A. (2016). Syntaxin-17 delivers PINK1/parkin-dependent mitochondrial vesicles to the endolysosomal system. J Cell Biol *214*, 275-291.

Mizushima, N., Yoshimori, T., and Ohsumi, Y. (2011). The role of Atg proteins in autophagosome formation. Annu Rev Cell Dev Biol *27*, 107-132.

Nguyen, T.N., Padman, B.S., Usher, J., Oorschot, V., Ramm, G., and Lazarou, M. (2016). Atg8 family LC3/GABARAP proteins are crucial for autophagosome-lysosome fusion but not autophagosome formation during PINK1/Parkin mitophagy and starvation. J Cell Biol *215*, 857-874.

Nishimura, T., Tamura, N., Kono, N., Shimanaka, Y., Arai, H., Yamamoto, H., and Mizushima, N. (2017). Autophagosome formation is initiated at phosphatidylinositol synthase-enriched ER subdomains. EMBO J *36*, 1719-1735.

Pattingre, S., Bauvy, C., and Codogno, P. (2003). Amino acids interfere with the ERK1/2-dependent control of macroautophagy by controlling the activation of Raf-1 in human colon cancer HT-29 cells. J Biol Chem *278*, 16667-16674.

Petiot, A., Ogier-Denis, E., Blommaart, E.F., Meijer, A.J., and Codogno, P. (2000). Distinct classes of phosphatidylinositol 3'-kinases are involved in signaling pathways that control macroautophagy in HT-29 cells. J Biol Chem *275*, 992-998.

Pilli, M., Arko-Mensah, J., Ponpuak, M., Roberts, E., Master, S., Mandell, M.A., Dupont, N., Ornatowski, W., Jiang, S., Bradfute, S.B.*, et al.* (2012). TBK-1 Promotes Autophagy-Mediated Antimicrobial Defense by Controlling Autophagosome Maturation. Immunity *37*, 223-234.

Popoff, V., Adolf, F., Brugger, B., and Wieland, F. (2011). COPI budding within the Golgi stack. Cold Spring Harb Perspect Biol *3*, a005231.

Saitoh, T., Fujita, N., Hayashi, T., Takahara, K., Satoh, T., Lee, H., Matsunaga, K., Kageyama, S., Omori, H., Noda, T.*, et al.* (2009). Atg9a controls dsDNA-driven dynamic translocation of STING and the innate immune response. Proc Natl Acad Sci U S A *106*, 20842-20846.

Seglen, P.O., and Gordon, P.B. (1984). Amino acid control of autophagic sequestration and protein degradation in isolated rat hepatocytes. J Cell Biol *99*, 435-444.

Seglen, P.O., Luhr, M., Mills, I.G., Saetre, F., Szalai, P., and Engedal, N. (2015). Macroautophagic cargo sequestration assays. Methods *75*, 25-36.

Shevchenko, A., Wilm, M., Vorm, O., and Mann, M. (1996). Mass spectrometric sequencing of proteins silver-stained polyacrylamide gels. Analytical chemistry *68*, 850-858.

Soreng, K., Munson, M.J., Lamb, C.A., Bjorndal, G.T., Pankiv, S., Carlsson, S.R., Tooze, S.A., and Simonsen, A. (2018). SNX18 regulates ATG9A trafficking from recycling endosomes by recruiting Dynamin-2. EMBO Rep.

Steegmaier, M., Oorschot, V., Klumperman, J., and Scheller, R.H. (2000). Syntaxin 17 is abundant in steroidogenic cells and implicated in smooth endoplasmic reticulum membrane dynamics. Mol Biol Cell *11*, 2719-2731.

Steegmaier, M., Yang, B., Yoo, J.S., Huang, B., Shen, M., Yu, S., Luo, Y., and Scheller, R.H. (1998). Three novel proteins of the syntaxin/SNAP-25 family. J Biol Chem *273*, 34171-34179.

Szalai, P., Hagen, L.K., Saetre, F., Luhr, M., Sponheim, M., Overbye, A., Mills, I.G., Seglen, P.O., and Engedal, N. (2015). Autophagic bulk sequestration of cytosolic cargo is independent of LC3, but requires GABARAPs. Exp Cell Res *333*, 21-38.

Takats, S., Glatz, G., Szenci, G., Boda, A., Horvath, G.V., Hegedus, K., Kovacs, A.L., and Juhasz, G. (2018). Non-canonical role of the SNARE protein Ykt6 in autophagosome-lysosome fusion. PLoS Genet *14*, e1007359.

Takats, S., Nagy, P., Varga, A., Pircs, K., Karpati, M., Varga, K., Kovacs, A.L., Hegedus, K., and Juhasz, G. (2013). Autophagosomal Syntaxin17-dependent lysosomal degradation maintains neuronal function in Drosophila. J Cell Biol *201*, 531-539.

Thurston, T.L., Ryzhakov, G., Bloor, S., von Muhlinen, N., and Randow, F. (2009). The TBK1 adaptor and autophagy receptor NDP52 restricts the proliferation of ubiquitin-coated bacteria. Nat Immunol *10*, 1215-1221.

Wang, Z., Miao, G., Xue, X., Guo, X., Yuan, C., Wang, Z., Zhang, G., Chen, Y., Feng, D., Hu, J.*, et al.* (2016). The Vici Syndrome Protein EPG5 Is a Rab7 Effector that Determines the Fusion Specificity of Autophagosomes with Late Endosomes/Lysosomes. Mol Cell *63*, 781-795.

Wild, P., Farhan, H., McEwan, D.G., Wagner, S., Rogov, V.V., Brady, N.R., Richter, B., Korac, J., Waidmann, O., Choudhary, C.*, et al.* (2011). Phosphorylation of the autophagy receptor optineurin restricts Salmonella growth. Science *333*, 228-233.

Young, A.R., Chan, E.Y., Hu, X.W., Kochl, R., Crawshaw, S.G., High, S., Hailey, D.W., Lippincott-Schwartz, J., and Tooze, S.A. (2006). Starvation and ULK1-dependent cycling of mammalian Atg9 between the TGN and endosomes. J Cell Sci *119*, 3888-3900.

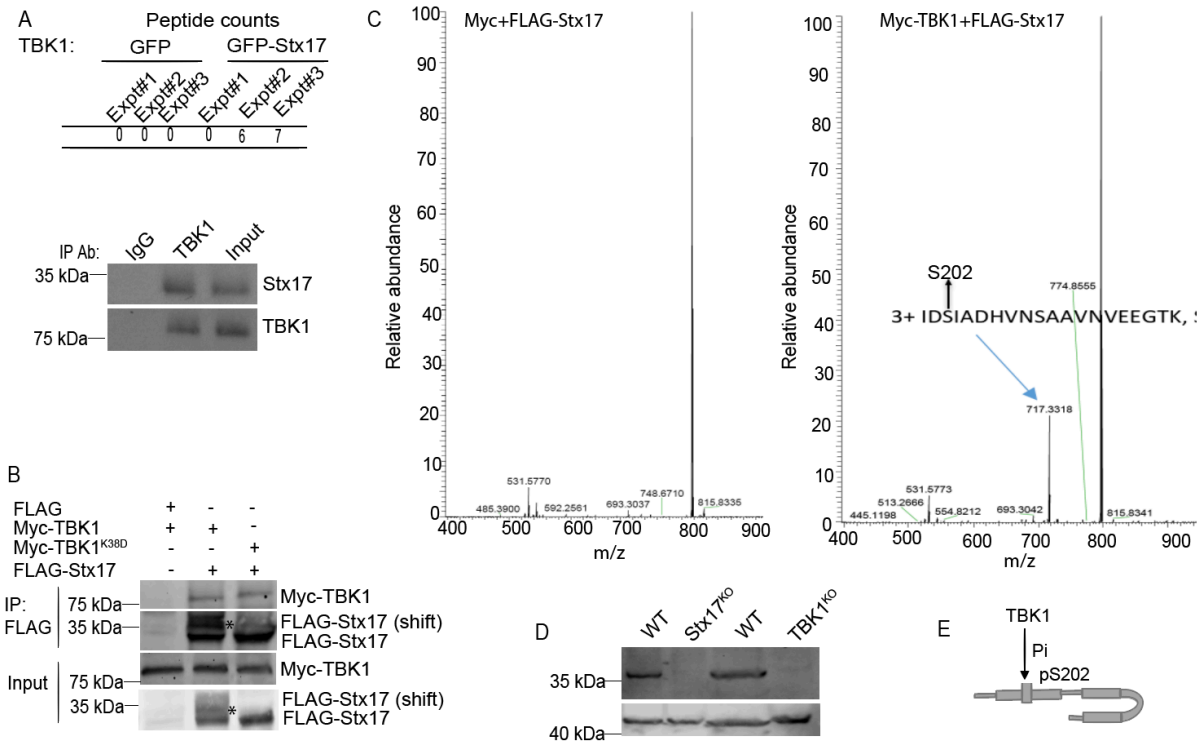

Figure 1. TBK1 interacts with and phosphorylates Stx17 at Ser-202. (A) MS analysis showing comparison of GFP or GFP-Stx17 peptides in co-IPs with TBK1, extracted from Table S1(upper panel). Co-IP between endogenous Stx17 and TBK1 in 293T cells (lower panel). **(B)** Co-IP of FLAG-Stx17 with Myc-TBK1^{WT} or Myc-TBK1^{K38D} in 293 T cells. * indicates the phospho-shift in FLAG-Stx17 induced by Myc-TBK1^{WT} (lane 2) and not by Myc-TBK1^{K38D} (lane 3). **(C)** Mass-spec analysis showing phosphorylation of FLAG-Stx17 at Ser-202 residue induced by Myc-TBK1 (right panel) and not by Myc alone (left panel). **(D)** Western blot showing expression of Stx17^{pS202} in in WT, Stx17^{KO} and TBK1^{KO} HeLa cells treated with 500ng/ml of LPS for 4h. **(E)** Schematic showing phosphorylation of Stx17 at Ser-202 residue by TBK1.

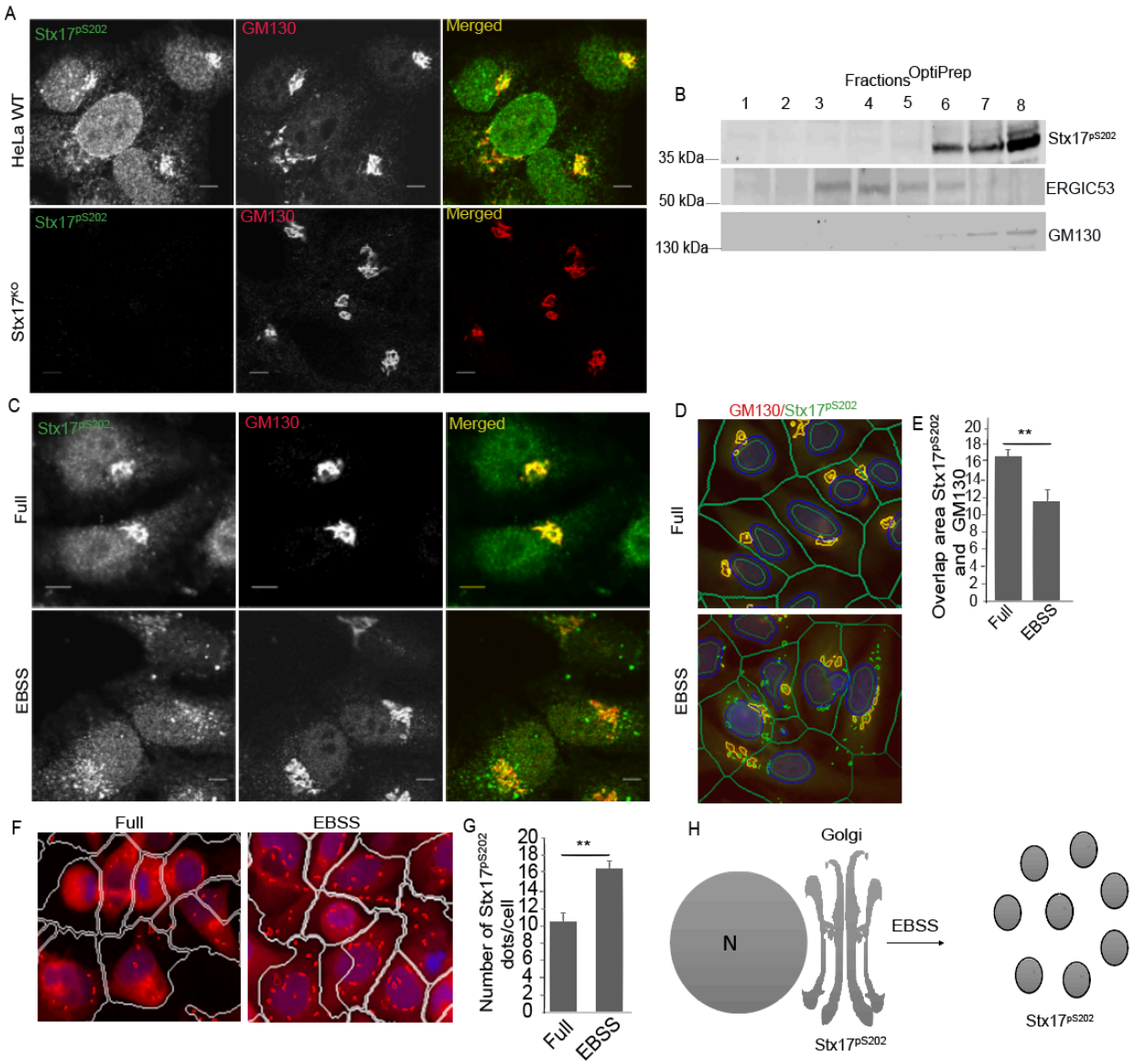

Figure 2. Stx17^{pS202} is localized in the Golgi. (A) Confocal microscopy showing colocalization between Stx17^{pS202} and GM130 in WT (upper panel) or Stx17^{KO} HeLa cells (lower panel). Scale bar 5 µm. **(B)** Membrane fractionation using OptiPrep gradients to analyze sub cellular fractionation of Stx17^{pS202}. **(C)** Confocal microscopy showing distribution of Stx17^{pS202} to peripheral puncta in response to starvation (Lower panel). Scale bar 5 µm. **(D, E)** High content microscopy of HeLa cells showing colocalization between Stx17^{pS202} and GM130 in full and starved conditions. **, $p < 0.01$, (n=3) t-test. **(F, G)** High content microscopy and quantification showing distribution of Stx17^{pS202} to peripheral puncta in response to autophagy induction by starvation. **, $p < 0.01$, (n=3) t-test. **(H)** A model showing translocation of Stx17^{pS202} from Golgi to peripheral puncta upon induction of autophagy with starvation.

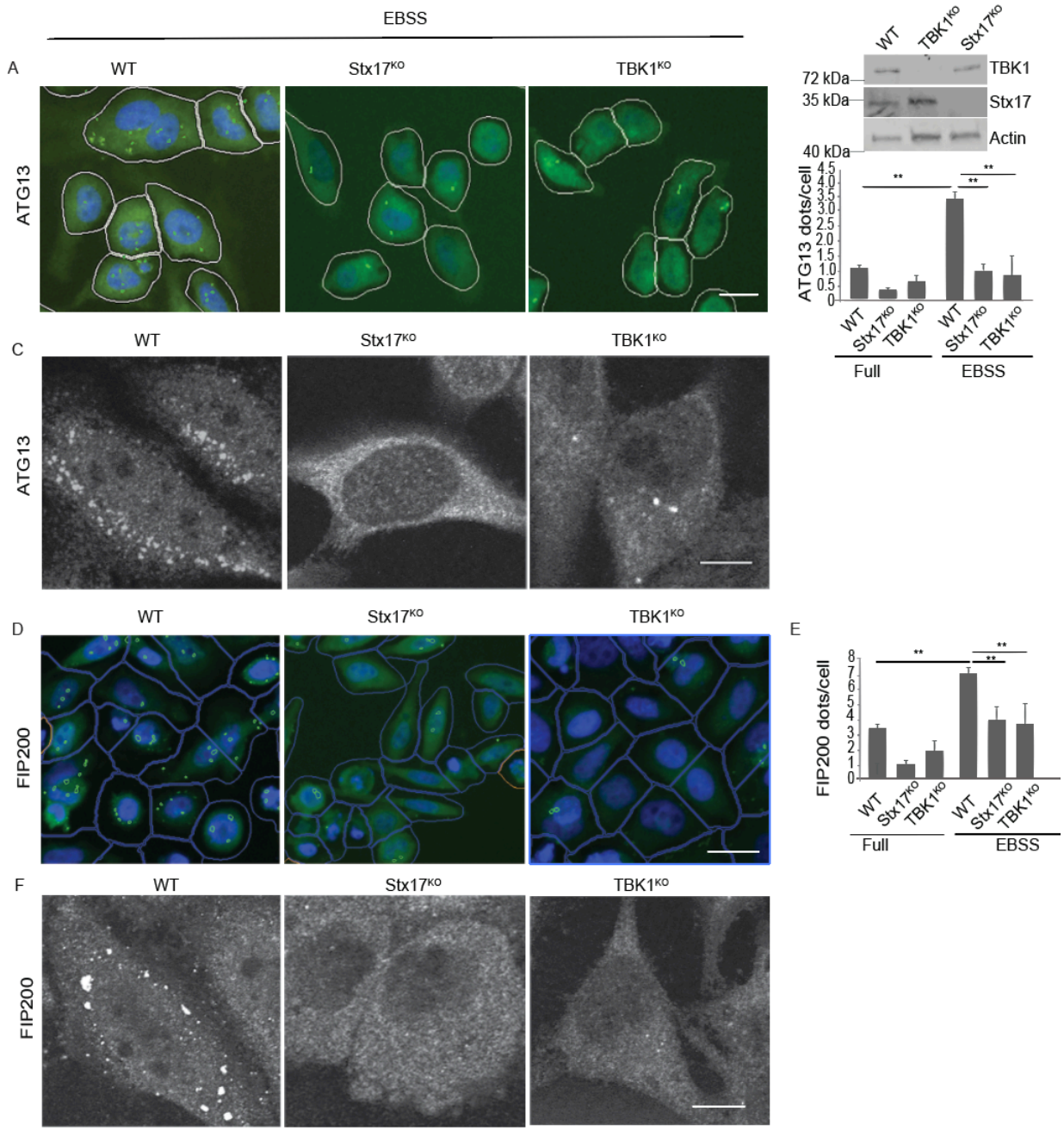

Figure 3. Stx17 and TBK1 are required for formation of mPAS. (A) High content microscopy showing the effect of Stx17 and TBK1 knock outs on formation of ATG13 puncta in HeLa cells. Masks; white: selected objects (cells); green: ATG13 positive dots. Western blot panel shows Stx17 and TBK1 knock outs in HeLa cells. Panel to the right, western blot showing TBK1 and Stx17 knock outs in HeLa cells. **(B)** High content quantifications showing the effect of Stx17 and TBK1 knock outs on formation of ATG13 puncta in HeLa cells. Scale bar 10 µm. **, $p < 0.01$, (n=3) ANOVA. **(C)** Confocal microscopy showing the effect of Stx17 and TBK1 knock outs on formation of ATG13 puncta in HeLa cells incubated in full media or induced for autophagy by incubation with EBSS for 1h. Scale bar 5 µm. **(D, E)** High content microscopy and quantifications showing

the effect of Stx17 and TBK1 knock outs on formation of FIP200 puncta in HeLa cells incubated in full media or EBSS for 1h. Scale bar 10 μm. **, $p < 0.01$, (n=3) ANOVA. **(F)** Confocal microscopy showing the effect of Stx17 and TBK1 knock outs on formation of FIP200 puncta in HeLa cells. Scale bar 5 μm.

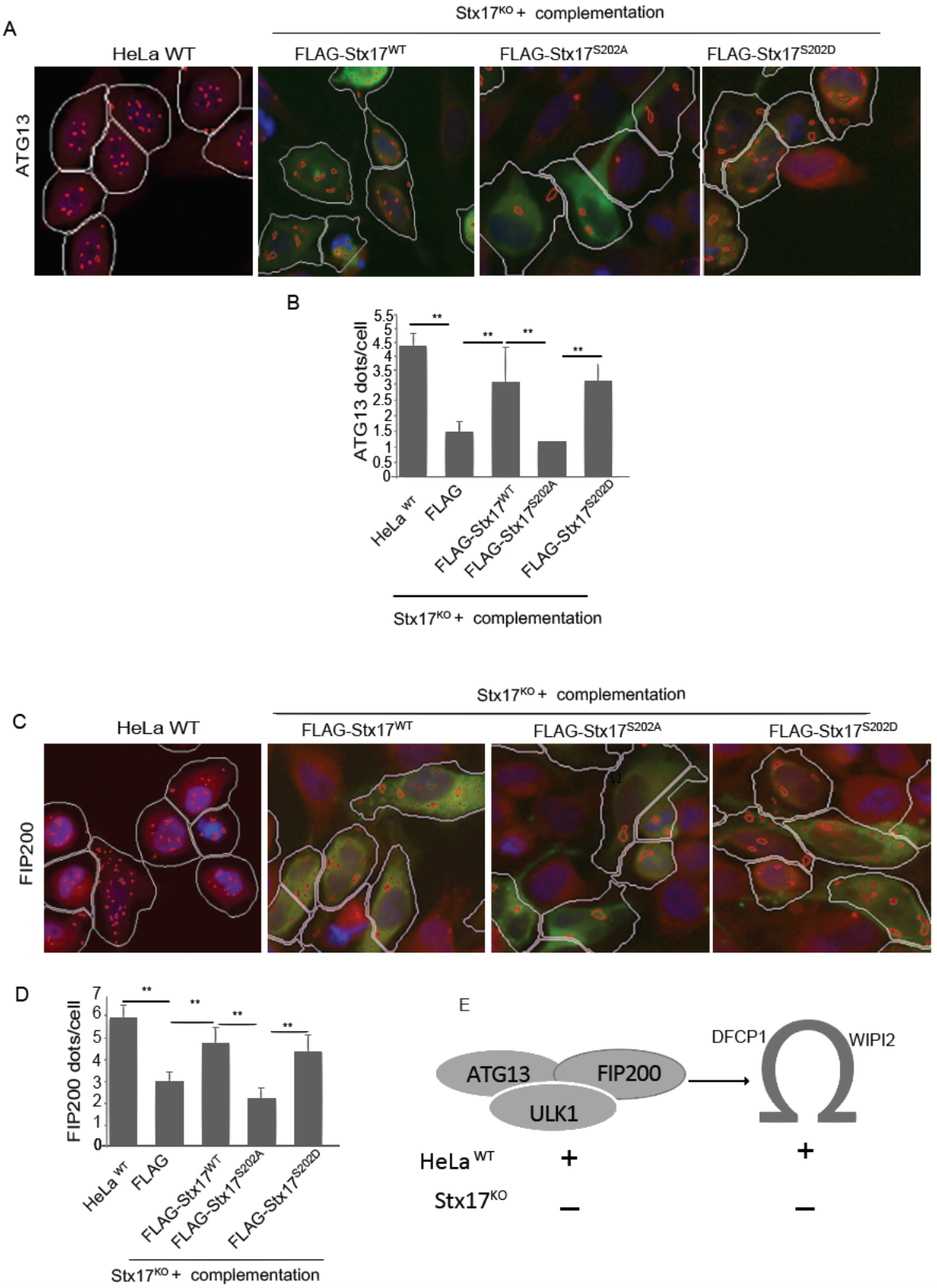

Figure 4. Phosphorylation of Stx17 by TBK1 is required for formation of ATG13 and FIP200 puncta. (A) Stx17^{KO} cells were transfected with FLAG-Stx17^{WT}, FLAG-Stx17^{S202A}

and FLAG-Stx17^{S202D} to complement the effect of Stx17 ^{KO} on ATG13 dot formation. Masks; white: FLAG positive cells, red: ATG13 dots in FLAG positive cells. HeLa WT (left) were left un-transfected for control. **(B)** High content quantifications showing the effect of complementation of Stx17 knock out cells with FLAG-Stx17^{WT}, FLAG-Stx17^{S202A} and FLAG-Stx17^{S202D} on formation of ATG13 puncta in HeLa cells incubated in full media or EBSS for 1h (Scale bar 10 μm). **, $p < 0.01$, (n=3) ANOVA. **(C)** Effect of complementation of Stx17^{KO} with FLAG-Stx17 ^{WT}, FLAG-Stx17^{S202A} and FLAG-Stx17^{S202D} on formation of FIP200 dots. Masks; white: FLAG positive cells, red: FIP200 puncta in FLAG positive cells. HeLa WT (left) were left un-transfected for control. **(D)** High content quantifications showing the effect of complementation of Stx17 knock out cells with FLAG-Stx17^{WT}, FLAG-Stx17^{S202A} and FLAG-Stx17^{S202D} on formation of FIP200 puncta in HeLa cells incubated in full media or EBSS for 1h. Scale bar 10 μm. **, $p < 0.01$, (n=3) ANOVA. **(E)** A model showing effect of Stx17 on formation of mammalian pre-autophagosomal structures (mPAS) and omegasomes.

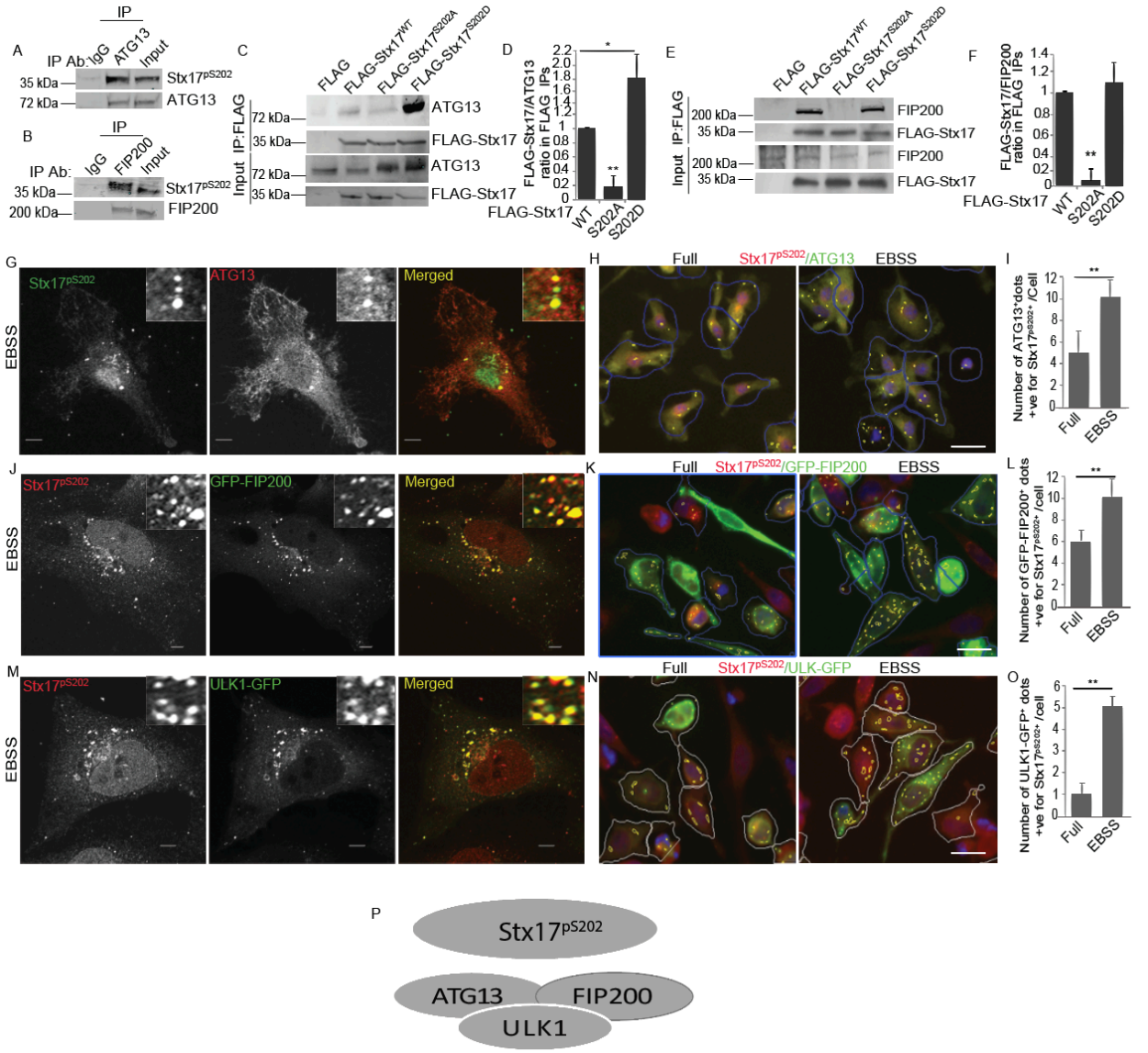

Figure 5. Stx17^{pS202} interacts with ATG13 and FIP200. (A, B) Co-IP showing interactions of endogenous ATG13 (A) or FIP200 (B) with Stx17^{pS202} in 293 T cells. **(C)** Co-IP analysis showing interactions between Stx17 WT, S202A or S202D with endogenous ATG13. **(D)** Graph showing quantifications of interactions between ATG13 and FLAG-Stx17 variants. **, $p < 0.01$, (n=3) ANOVA. **(E)** Co-IP analysis showing interactions between Stx17 WT, S202A or S202D with endogenous FIP200. **(F)** Graph showing quantifications between FIP200 and FLAG-Stx17 variants. **, $p < 0.01$, (n=3) ANOVA. **(G)** Confocal microscopy to show colocalization between endogenous ATG13 and Stx17^{pS202} in BMMs incubated with EBSS for 1h. Scale bar 5 µm. **(H,I)** High content microscopy and quantifications showing colocalization between ATG13 and Stx17^{pS202} in BMMs incubated in full media or induced for autophagy by incubation with EBSS for 1h . **, $p < 0.01$, (n=3) t-test. **(J)** Colocalization between GFP-FIP200 and Stx17^{pS202} in HeLa cells incubated with EBSS for 1h. **(K, L)** High content microscopy and quantifications showing colocalization between GFP-FIP200 and Stx17^{pS202} in HeLa cells transfected with GFP-FIP200 and incubated in full media or induced for autophagy by incubation with

EBSS for 1h. **, $p < 0.01$, (n=3) t-test. Masks; blue: GFP-FIP200 gated cells (pseudo color: GFP-FIP200 is red and Stx17^{pS202} is green); yellow: number of Stx17^{pS202} dots also positive for GFP-FIP200 dots. **(M)** Confocal microscopy showing colocalization between ULK1-GFP and Stx17^{pS202} in HeLa cells incubated with EBSS for 1h. **(N, O)** High content microscopy and quantifications showing colocalization between ULK1-GFP and Stx17^{pS202} in HeLa cells transfected with GFP-ULKL1 and incubated in full media or induced for autophagy by incubation with EBSS for 1h. **, $p < 0.01$, (n=3) t-test. Masks; white: ULK1-GFP positive objects cells; yellow: number of Stx17^{pS202} dots also positive for ULK1-GFP dots. **(P)** A model showing Stx17^{pS202} as an interacting partner of mPAS complex.

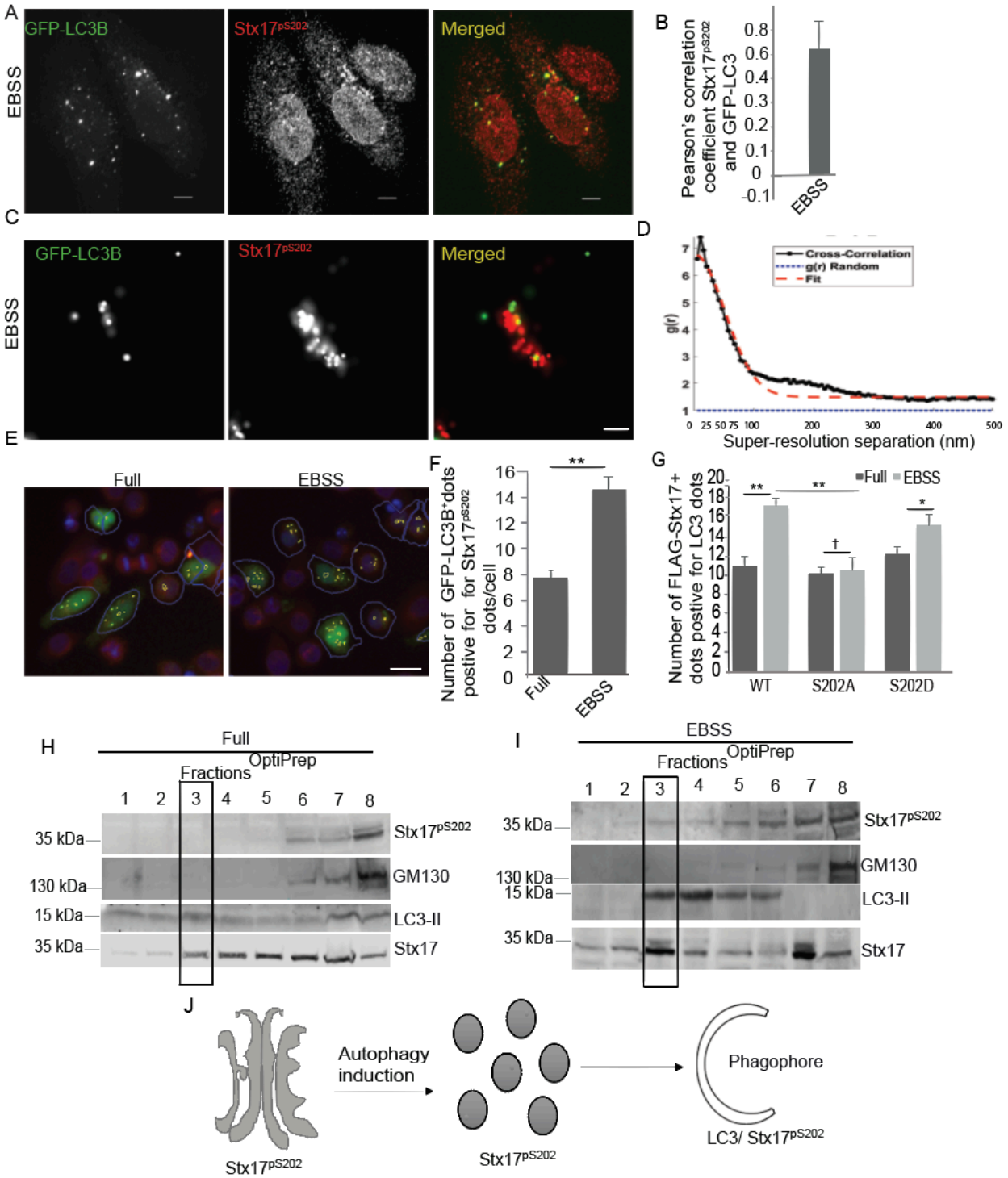

Figure 6. Stx17^{pS202} is on LC3-positive autophagosomes upon induction of autophagy. (A) Confocal microscopy showing colocalization between GFP-LC3B and Stx17^{pS202} in HeLa cells incubated with EBSS for 2h. Scale bar 5 µm. **(B)** Pearson's correlation coefficient (>20 cells) of colocalization between GFP-LC3B and Stx17^{pS202}**. (C, D)** Super-resolution microscopy showing colocalization between GFP-LC3B and Stx17^{pS202} in HeLa cells incubated with EBSS for 2h. Scale bar 500nm. **(E,F)** High content microscopy (HC) and quantifications showing colocalization between GFP-LC3B and

Stx17^{pS202} in HeLa cells incubated in full media or in EBSS for 2h. Scale bar 10 μm. **, $p < 0.01$, (n=3) t-test. **(G)** HC quantifications showing colocalization between FLAG-Stx17 WT, FLAG-Stx17 S202A and FLAG-Stx17 S202D with LC3 in HeLa cells incubated in full media or in EBSS for 2h. **, $p < 0.01$, (n=3) ANOVA. **(H, I)** Membrane fractions using OptiPrep gradients to test redistribution of Stx17^{pS202} from Golgi (H) in full media to LC3-II fraction in EBSS (I).

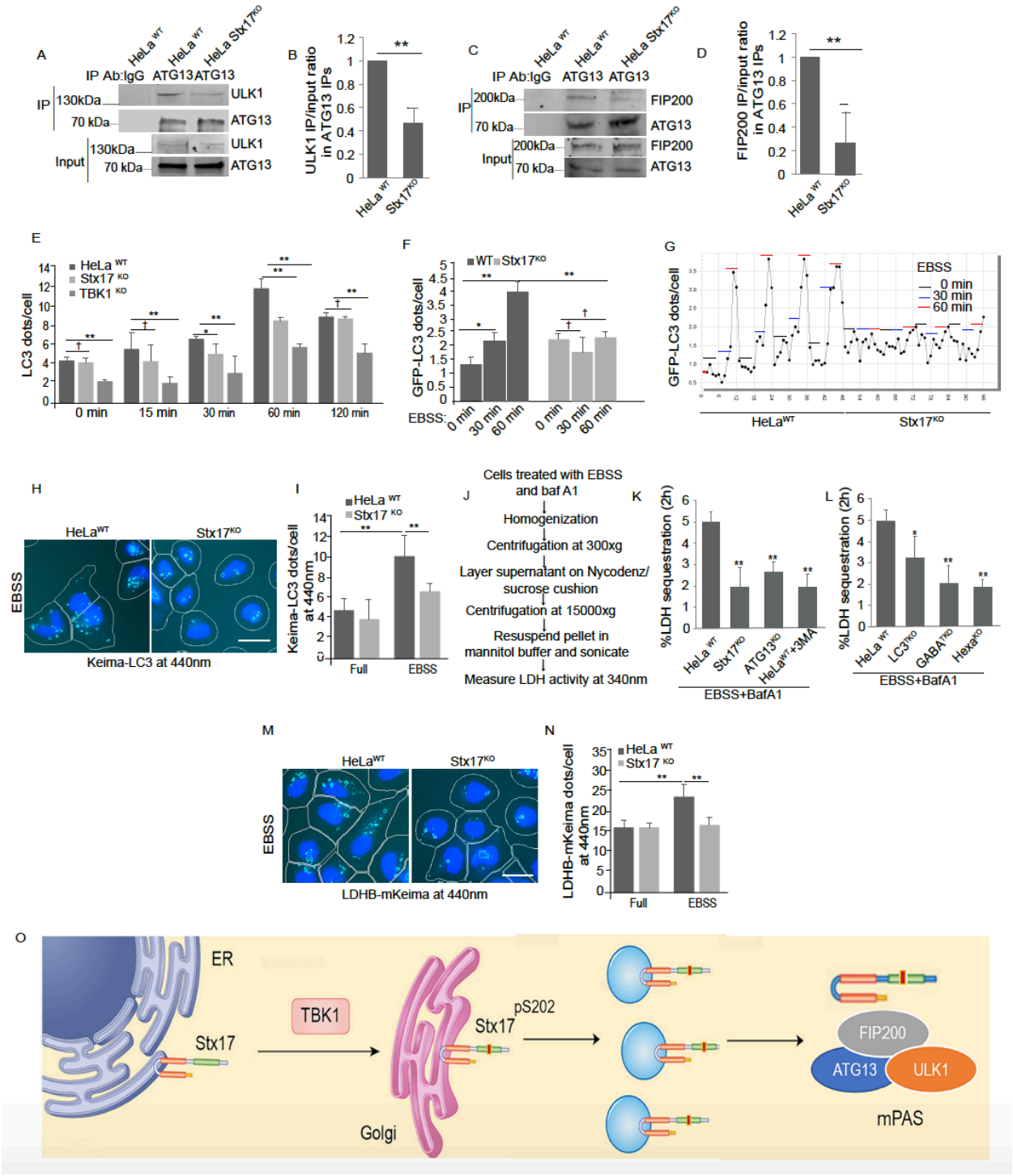

Figure 7: Stx17 is required for autophagy initiation. (A) Co-IP analysis of interactions between ATG13 and ULK1 in HeLa wild type or Stx17 knock out cells. **(B)** Graph showing quantification of IP/input ratio of ULK1 in Co-IP with ATG13 in HeLa wild type vs Stx17 knock outs. $p < 0.01$, (n=3) t-test. **(C)** Co-IP to test the effect of Stx17 knock out on interactions between FIP200 and ATG13. **(D)** Graph showing quantification of IP/input ratio of ATG13 in Co-IP with FIP200 in HeLa wild type vs Stx17 knock outs. $p < 0.01$, (n=3) t-test. **(E)** High content (HC) quantification showing effect of Stx17 and TBK1 knock

outs on formation of LC3 puncta in time dependent starvation response. *, p<0.05; **, p < 0.01, (n=3) ANOVA. (**F)** High content analysis to test the effect of Stx17 knock out on GFP-LC3 puncta formation after 30 min or 1h of starvation. *, p<0.05; **, p < 0.01, (n=3) ANOVA. **(G)** Screen shot of HC-scanned 96 well plate of HeLa cells transfected with mCherry-GFP-LC3B; EBSS incubation for 0 min, 30 min or 60 min; $HeLa^{WT}$ (left half of the plate) or in $Stx17^{KO}$ (right half of the plate). For each experimental point, a minimum of 500 valid object/cells per well were counted for GFP-LC3 puncta. **(H, I)** High content microscopy of Keima-LC3 fluorescence at 440nm in $HeLa^{WT}$ or $Stx17^{KO}$ cells incubated in full media or in EBSS for 6h.*, p<0.05; **, p < 0.01, (n=3) ANOVA. **(J)** Schematics showing different steps in LDH sequestration assay. **(K)** LDH sequestration assay showing the effect of Stx17 and ATG13 knock outs on LDH sequestration in cell induced for autophagy by incubation with EBSS for 2h in presence of bafilomycin A1. 3 methyladenine (10 mM) was used as a positive control. **(L)** LDH sequestration assay showing the effect of mATG8s knock outs on LDH sequestration in cells induced for autophagy by incubation with EBSS for 2h in presence of bafilomycin A1. **(M, N)** High content microscopy of LDH-keima fluorescence at 440nm in HeLa wt or $Stx17^{KO}$ cells incubated in full media or with EBSS for 2h.*, p<0.05; **, p < 0.01, (n=3) ANOVA. **(O)** Model showing Stx17 in ER membranes and moves to Golgi after its phosphorylation by TBK1. After induction of autophagy $Stx17^{pS202}$ translocates from Golgi to peripheral puncta and is associated with mPAS.

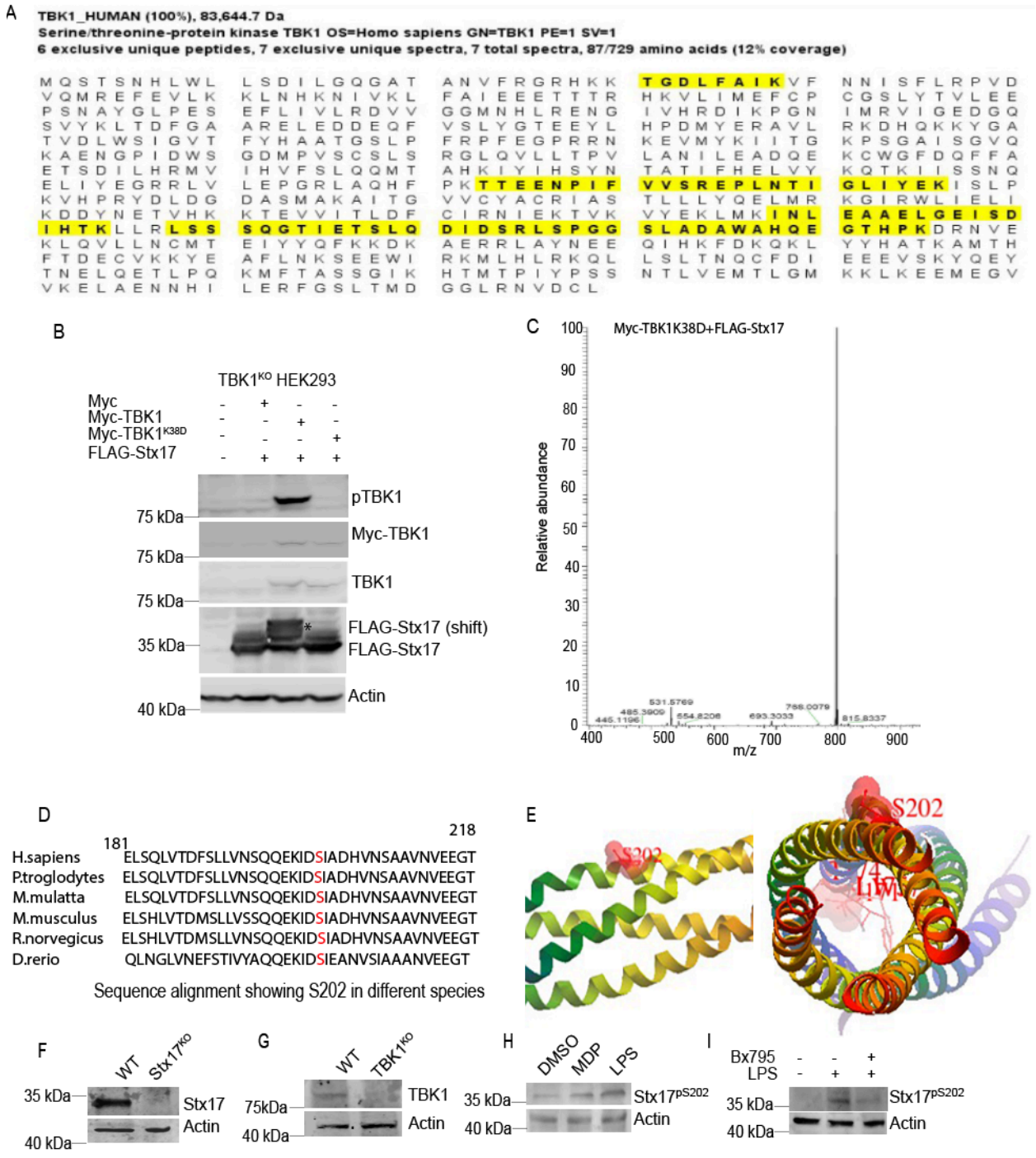

Figure S1, related to Figure 1. TBK1 phosphorylates Stx17. (A) Proteomics data showing number of TBK1 peptides interacting with GFP-Stx17**. (B)** Western blot from cells expressing Myc, Myc-TBK1^{WT} or Myc-TBK1^{K38D} with FLAG-Stx17. "*" represents phosphorylation-induced shift. **(C)** Mass spectrometry analysis showing the effect of Myc-TBK1^{K38D} on FLAG-Stx17 phosphorylation (related to Figure 1C). **(D)** Sequence alignment showing conserved S202 residue in Stx17 from human to fish. **(E)** Crystal structure from database showing location of S202 in Stx17**. (F)** Western blot confirming

Stx17 knock out in $Stx17^{KO}$ HeLa cells**. (G)** Western blot showing TBK1 knock out in $TBK1^{KO}$ HeLa cells**. (H)** Western blot showing effect of MDP or LPS on expression of $Stx17^{pS202}$ in HeLa cells**. (I)** Western blot showing effect of TBK1 inhibitor BX795 on LPS induced expression of $Stx17^{pS202}$ in HeLa cells**.**

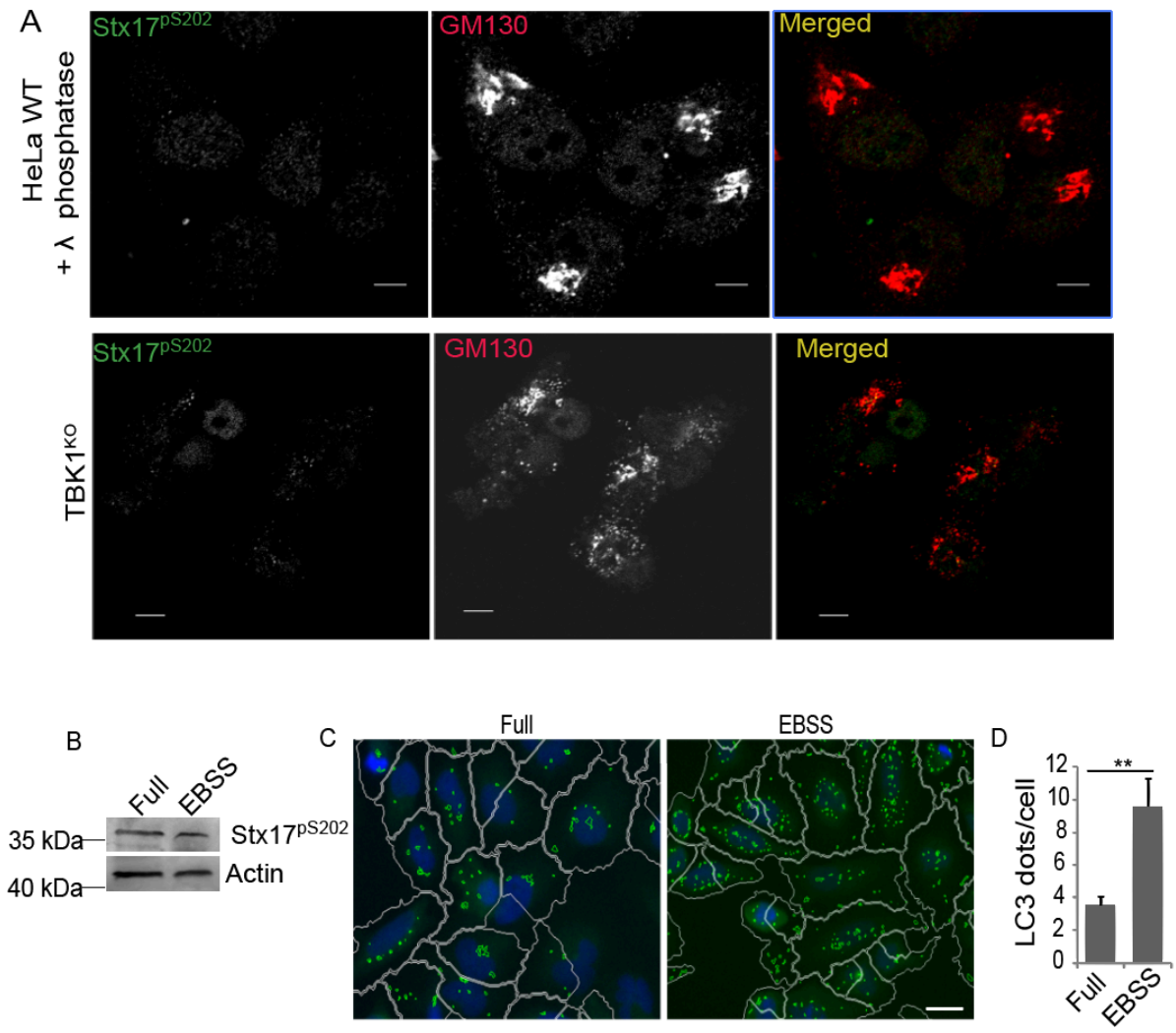

Figure S2, related to Figure 2. Stx17^{pS202} is localized in Golgi. (A) Colocalization between Stx17^{pS202} and GM130 in HeLa cells treated with ƛ phosphatase (upper panel) and in TBK1^{KO} cells (lower panel). Scale bar 5 µm. **(B-D)** Western blot showing effect of starvation (2h EBSS) induced autophagy (as shown by induction of LC3 puncta in C,D) on levels of Stx17^{pS202}. **, $p < 0.01$, (n=3) t-test.

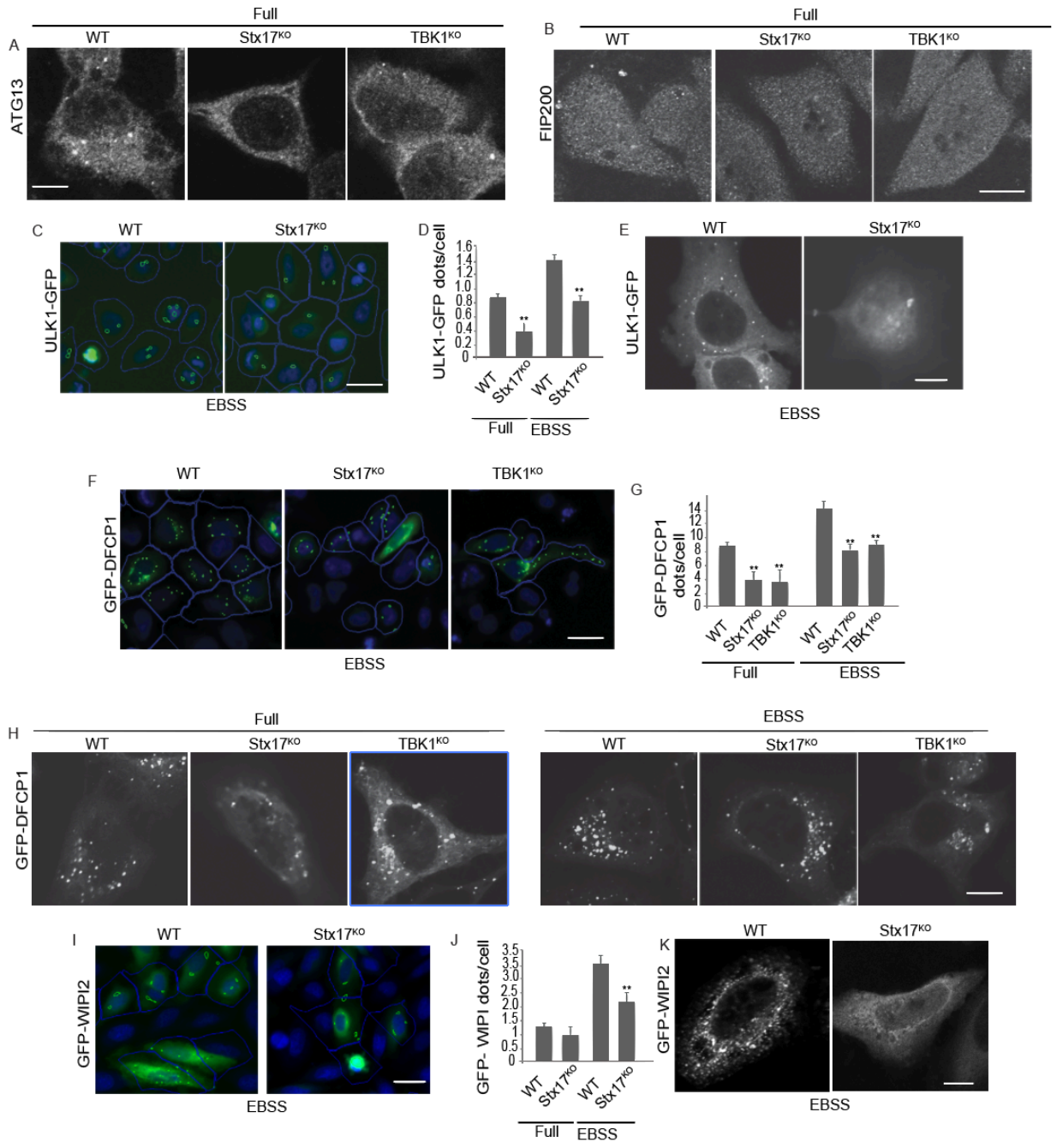

Figure S3, related to Figure 3. Stx17 and TBK1 are required for formation of pre-autophagosomal structures. (A, B) Confocal microscopy showing ATG13 and FIP200 dots in HeLa^{WT}, Stx17^{KO} and TBK1^{KO} cells in full media. Scale bar 5 µm. **(C, D)** High content analysis showing effect of Stx17^{KO} on formation of ULK1-GFP dots in full media or cells induced for autophagy by incubating in EBSS for 1h. **, $p < 0.01$, (n=3) ANOVA. Masks; blue: gated GFP^{+} cells; green: ULK1-GFP^{+} dots. **(E)** Confocal microscopy to analyze the effect of Stx17 knock out on formation of ULK1-GFP dots. Scale bar 5 µm. **(F)** Confocal microscopy to analyze the effect of Stx17 and TBK1 knock outs on formation of GFP-DFCP1 dots. **(G, H)** High content microscopy and quantifications showing effect of Stx17 and TBK1 knock outs on formation of GFP-DFCP1 dots in cells incubated in full

media or induced for autophagy by incubating in EBSS for 1h. **, $p < 0.01$, (n=3) ANOVA. Masks; blue: gated GFP^+ cells; green: GFP-$DFCP1^+$ dots. **(I, J)** High content analysis showing effect of $Stx17^{KO}$ on formation of GFP-WIPI2 dots in full media or cells induced for autophagy by incubating in EBSS for 1h. **, $p < 0.01$, (n=3) ANOVA. Masks; blue: gated GFP^+ cells; green: GFP-$WIPI2^+$ dots. **(K)** Confocal microscopy to analyze the effect of Stx17 and TBK1 knock outs on formation of GFP-WIPI2 dots.

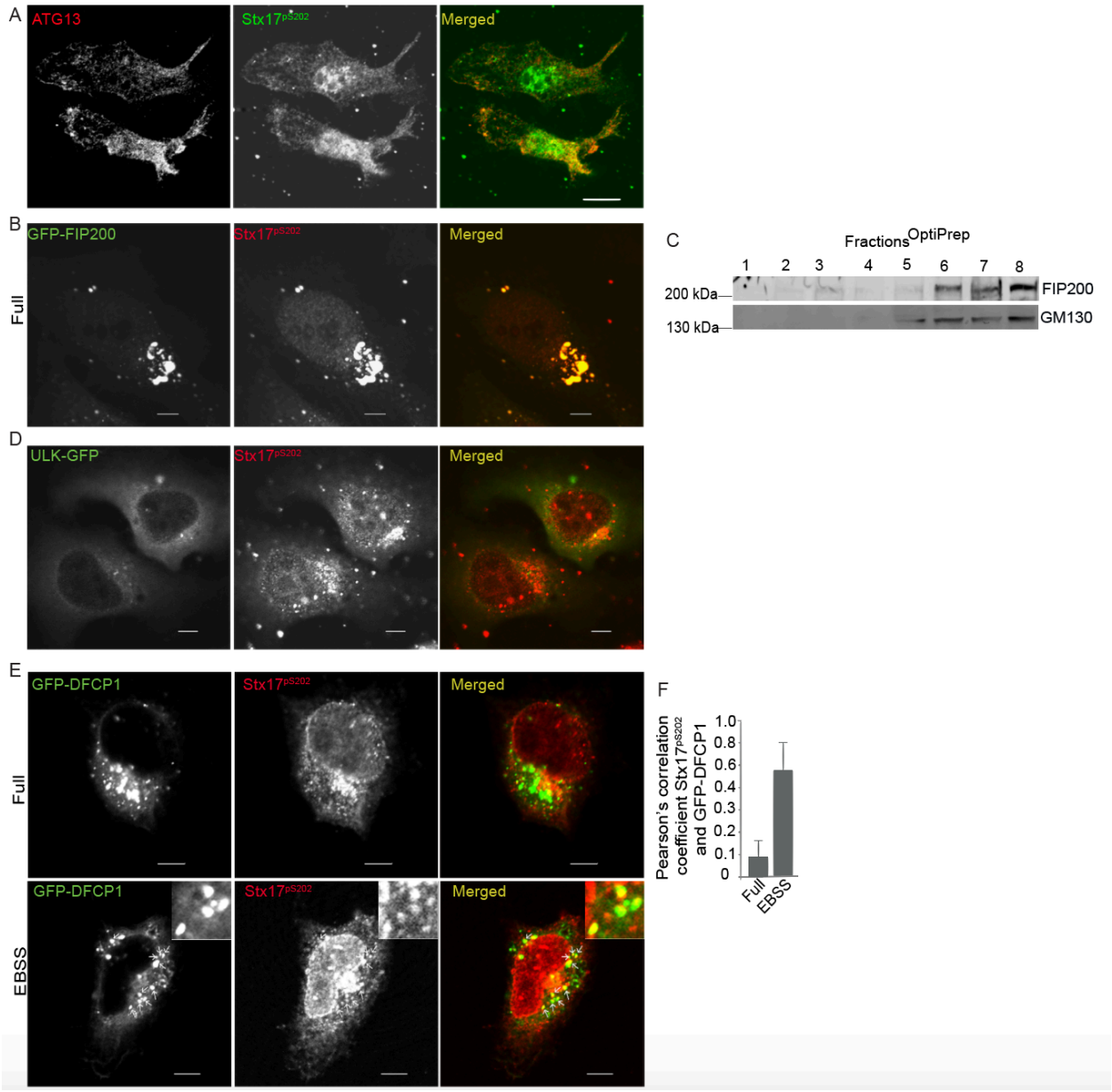

Figure S4, related to Figure 5. Stx17^{pS202} colocalizes with mPAS. (A) Confocal microscopy to analyze colocalization between Stx17^{pS202} and ATG13 in mouse BMMs incubated in full media. Scale bar 5 μm. **(B)** Confocal microscopy to analyze colocalization between Stx17^{pS202} and GFP-FIP200 in HeLa cells incubated in full media. Scale bar 5 μm. **(C)** Western blot from Optiprep gradients showing FIP200 co-fractionation with Golgi marker GM130. **(D)** Confocal microscopy to analyze colocalization between Stx17^{pS202} and ULK1-GFP in HeLa cells incubated in full media. Scale bar 5 μm. **(E)** Confocal microscopy to analyze colocalization between Stx17^{pS202} and GFP-DFCP1 in HeLa cells incubated in full media (upper panel) or in EBSS for 1h (lower panel). Arrows show Stx17^{pS202} and GFP-DFCP1 dots overlapping with each other. Scale bar 5 μm. **(F)** Pearson's correlation coefficient (>20 cells) of colocalization between GFP-DFCP1 and Stx17^{pS202}.

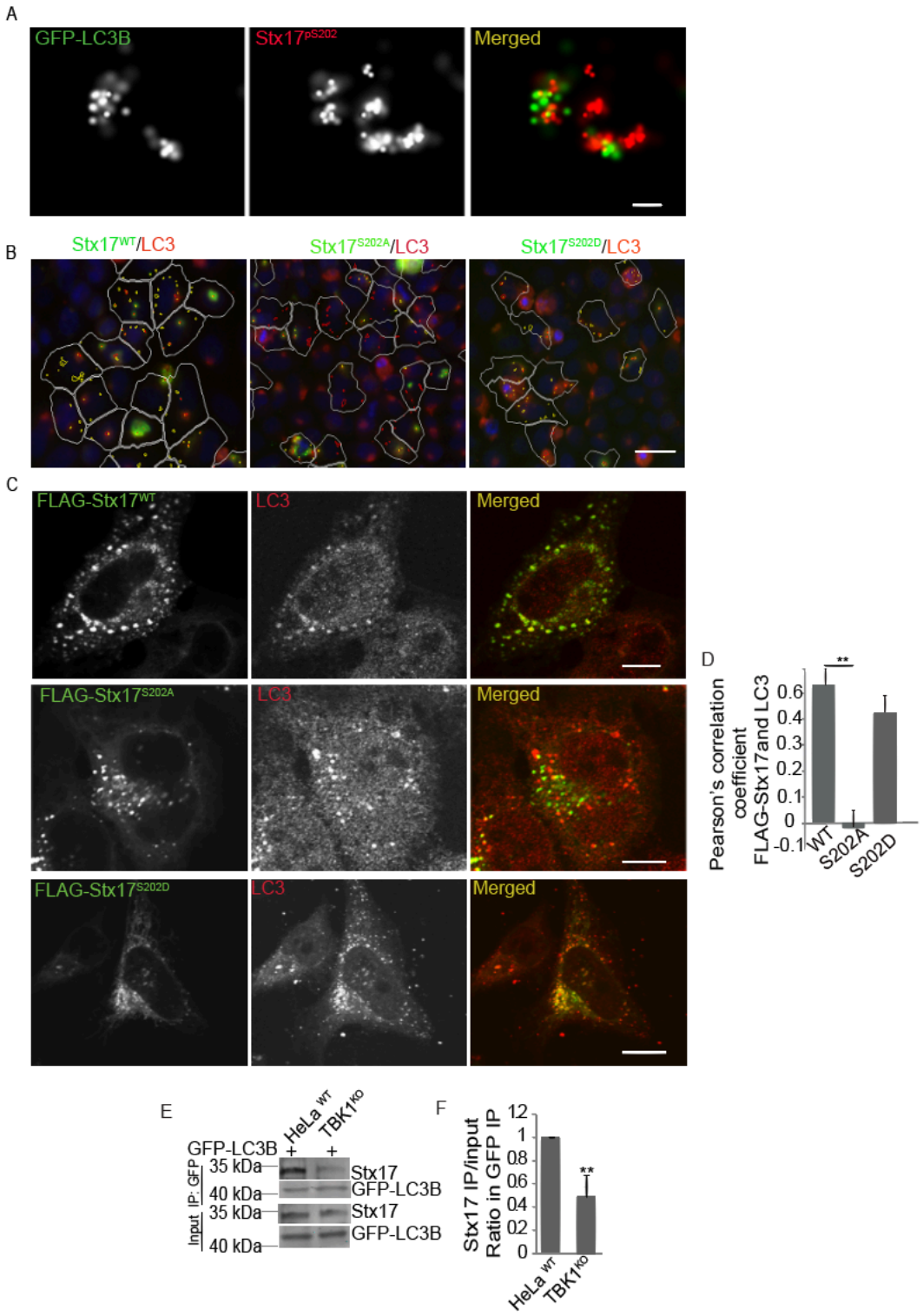

Figure S5, related to Figure 6. WT and phosphomimetic but not non-phosphorylatable Stx17 colocalizes with LC3. (A) Super-resolution microscopy showing colocalization between Stx17^{pS202} and GFP-LC3B in cell induced for autophagy with EBSS for 2h. Scale bar 500nm. **(B)** High content microscopy imaging showing

colocalization between FLAG-tagged Stx17WT, S202A or S202D mutants with LC3 in cell induced for autophagy with starvation. **(C)** Confocal Microscopy showing colocalization between FLAG tagged Stx17WT, S202A or S202D mutants with LC3 in cell induced for autophagy with starvation. Scale bar 5 μm. **(D)** Graph showing Pearson's correlation coefficient of colocalization between FLAG-tagged Stx17 variants and LC3. (E, F) Co-IP analysis and quantifications showing effect of TBK1 knock out on interactions between Stx17 and GFP-LC3B. $p<0.05$; **, $p < 0.01$, (n=3) t-test.

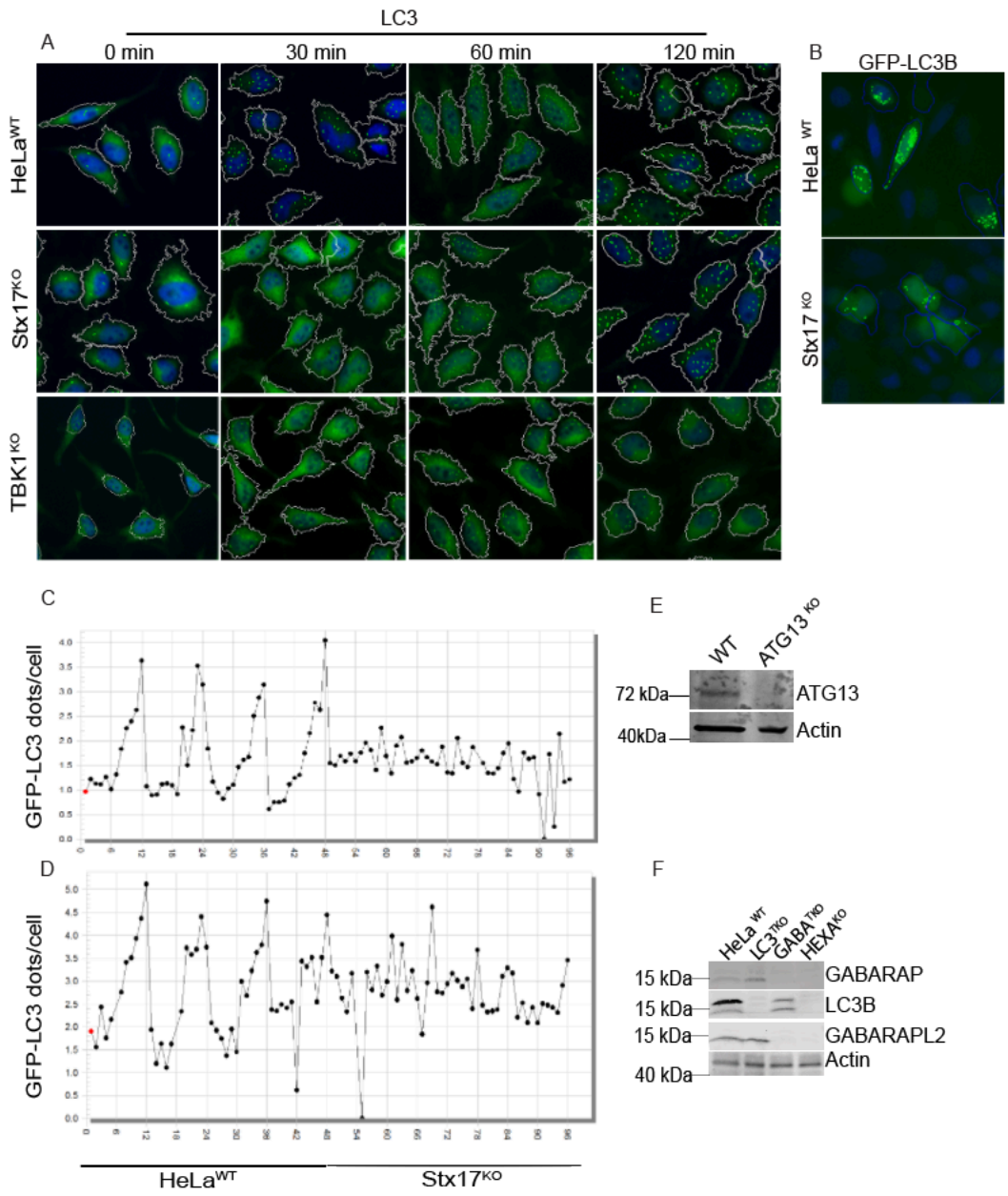

Figure S6, related to Figure 7. Stx17 regulates autophagy initiation (A) High content microscopy showing effect of Stx17 and TBK1 knock out on LC3 puncta formation at indicated time points of autophagy induction by starvation. **(B)** High content images showing effect of Stx17 knock out on GFP-LC3 puncta formation after 1h autophagy induction with EBSS. **(C, D)** Screenshots of layout of the plates used in Figures 7F and S7B, showing effect of Stx17 knock outs (right half of the plates) on formation of LC3 puncta. **(E)** Western blot showing ATG13 knock out in HeLa cells. **(F)** Western blot confirming LC3B, GABRAP and GABARAPL2 knock outs in mATG8s knock out cells.